LAPPEENRANTA UNIVERSITY OF TECHNOLOGY
DEPARTMENT OF ELECTRICAL ENGINEERING

EFFECTS OF VACANCY-TYPE DEFECTS IN SILICON BASED PARTICLE DETECTORS

The supervisor of this study was Professor Matti Alatalo and the examiner was PhD Christopher D. Latham.

Lappeenranta 9.5.2008

Pekka Neuvonen
Korpimetsänkatu 5 B 7
53850 Lappeenranta

ABSTRACT

Author: Neuvonen, Pekka Tapio

Subject: **EFFECTS OF VACANCY-TYPE DEFECTS IN SILICON BASED PARTICLE DETECTORS**

Department: Department of electrical engineering

Year: 2008

Place: Lappeenranta

Lappeenranta University of Technology, Master's Thesis, 51 pages, 20 figures and 1 table.

Supervisor: Professor Matti Alatalo

Examiner: PhD. Christopher D. Latham

Keywords: Particle detectors, Silicon, Defects, Radiation

The semiconductor particle detectors used at CERN experiments are exposed to radiation. Under radiation, the formation of lattice defects is unavoidable. The defects affect the depletion voltage and leakage current of the detectors, and hence affect on the signal-to-noise ratio of the detectors. This shortens the operational lifetime of the detectors. For this reason, the understanding of the formation and the effects of radiation induced defects is crucial for the development of radiation hard detectors.

In this work, I have studied the effects of radiation induced defects—mostly vacancy related defects—with a simulation package, S . Thus, this work essentially concerns the effects of radiation induced defects, and native defects, on leakage currents in particle detectors.

Impurity donor atom-vacancy complexes have been proved to cause insignificant increase of leakage current compared with the trivacancy and divacancy-oxygen centres. Native defects and divacancies have proven to cause some of the leakage current, which is relatively small compared with trivacancy and divacancy-oxygen.

TIIVISTELMÄ

Tekijä: Neuvonen, Pekka Tapio

Nimi: **EFFECTS OF VACANCY-TYPE DEFECTS IN SILICON BASED PARTICLE DETECTORS**

Osasto: Sähkötekniikan osasto

Vuosi: 2008

Paikka: Lappeenranta

Lappeenrannan teknillinen yliopisto, Diplomityö, 51 sivua, 20 kuvaa ja 1 taulukko.

Ohjaaja: Professori Matti Alatalo

Tarkastaja: PhD. Christopher D. Latham

Hakusanat: Hiukkasilmaisimet, Pii, Hilavirhe, Säteily

Puolijohdehiukkasilmaisimet, joita käytetään CERN:in kokeissa, altistuvat säteilylle. Säteily muodostaa ilmaisimiin hilavirheitä, jotka vaikuttavat ilmaisimen tyhjennysjännitteeseen sekä vuotovirtaan, ja siten myös signaalin ja kohinan suhteeseen. Tämä johtaa väājäämättä ilmaisimen toimintaiän lyhenemiseen. Jotta voidaan kehittää säteilyn kestäviä hiukkasilmaisimia, on ymmärrettävä säteilyn aiheuttamien hilavirheiden synty sekä niiden vaikutukset.

Tässä työssä on tutkittu lähinnä vakansseihin liittyviä säteilyn aiheuttamia hilavirheitä Silvaco-ohjelmistolla. Tutkimus keskittyy lähinnä säteilyn aiheuttamien hilavirheiden vaikutukseen vuotovirtaan.

Epäpuhtausatomien ja vakanssien muodostamien kompleksien on havaittu aiheuttavan vain vähäistä kasvua vuotovirtaan, verrattaessa niitä kolmoisvakanssiin ja kaksoisvakanssihappi yhdistelmiin. Alkuperäiset hilavirheet, sekä kaksoisvakanssin on todistettu aiheuttavan vuotovirran kasvua, mutta kuitenkin huomattavasti vähäisemmissä määrin, kuin kolmoisvakanssin sekä kaksoisvakanssi-happi yhdistelmän.

PREFACE

This thesis was written for the Department of Electrical Engineering at Lappeenranta University of Technology.

I would like to acknowledge my supervisor, Professor Matti Alatalo, for the opportunity he gave me, his help, and his guidance. I also would like to thank the Examiner of this thesis, Dr. Chistopher Latham, for his tremendous help in both, physics and language. I also would like to thank the rest of the members in our laboratory for their help in practical matters.

I thank my friends for their support and the possibility to spend my free time with them. Finally, I would like to thank my family for their support throughout my studies.

Contents

1 Introduction **6**

2 Atoms **7**

2.1 Band Structure . . . 9
2.2 Conductivity . . . 10
2.2.1 Charge carrier mobility . . . 11
2.3 Semiconductors . . . 11
2.3.1 *N*-type extrinsic semiconductor . . . 12
2.3.2 *P*-type extrinsic semiconductor . . . 13
2.4 Defects . . . 13
2.4.1 Point defects . . . 13
2.4.2 Dislocations . . . 14
2.4.3 Plane defects . . . 16

3 Semiconductor particle detectors **16**

3.1 P-n junction . . . 17
3.2 Operation principle . . . 20
3.3 Leakage current . . . 21
3.4 Strip Detectors . . . 22
3.5 Pixel detectors . . . 23
3.6 Radiation induced damage . . . 24
3.6.1 Vacancies . . . 25
3.6.2 Vacancy-oxygen complexes . . . 28
3.6.3 *E*-centers, Carbon and minority defects . . . 31

4 Simulation program **32**

4.1 Athena . . . 32
4.2 Atlas . . . 33

5 Simulations **33**

5.1 Diode structure . . . 34
5.2 Defect parameters . . . 35

6 Results **38**

6.1 As_2V and PV . . . 38
6.2 Divacancy and C_iO_i . . . 39
6.3 Divacancy-Oxygen and trivacancy . . . 41

7 Conclusions **46**

REFERENCES **48**

ABBREVIATIONS

ϵ	Dielectric constant
$\varepsilon_{c,v}$	Conduction and valence band edge
Λ	Volume of space charge region
μ	Chemical potential
$\mu_{e,h}$	Mobility for electrons and holes
$\rho(x)$	Charge distribution as a function of location
σ	Conductivity
τ	Generation lifetime
ϕ	Potential
$\phi(x)$	Potential as a function of location
A	Atomic mass
A	Area
$a_{u,g}$	Electron energy levels
bcc	Body centred cubic
BD	Bistable Donor
CCE	Charge collection efficiency
CERN	Conseil Européen pour la Recherche Nucléaire
CID	Current injected detector
CMS	Compact Muon Solenoid
Cz	Czochralski silicon
degen	Degeneration
DFT	Density Functional Theory
DLTS	Deep Level Transient Spectroscopy

$d_{n,p}$	Lengths of n-type and p-type regions
DOFZ	Diffuse oxygenated float zone silicon
E	Energy
e	Electron charge
$E_{C,V}$	Conduction and valence band edges
E_g	Width of band gap
E_p	Formation energy of electron-hole pair
$e_{u,g}$	Electron energy levels
F	Fano factor
fcc	face centered cubic
FZ	Float zone silicon
hcp	hexagonal close packed
I	Current
IC	Integrated Circuit
I_g	Leakage current
J	Current density
k_{B}	Boltzmann constant
l	Azimuthal or angular momentum
LHC	Large Hadron Collider
m_l	Magnetic quantum number
N	Number of neutrons
n	Principal quantum number
n	Number of charge carriers
$N_a(x)$	Acceptor density as a function of location

$n_c(x)$	Electron density as a function of location
$N_d(x)$	Donor density as a function of location
N_eff	Effective doping concentration
n_i	Intrinsic carrier concentration
p	Number of holes
PKA	Primary knock-on atom
$p_v(x)$	Hole density as a function of location
Q_s	Collected charge
rms	Root mean square
SCR	Space Charge Region
sign	Capture cross section for electrons
sigp	Capture cross section for holes
T	Temperature
TD	Thermal Donor
v_d	Drift velocity
x	Location on x-axel in cartesian coordinates
Z	Atomic number

1 Introduction

Modern material science and physics have arrived at a point that requires scientists to study ever smaller particles. For this purpose *Conseil Européen pour la Recherche Nucléaire* (CERN) was created in 1952. Its purpose is to study basic properties of matter, and the forces that hold it together. CERN is located near Geneva, on the border of France and Switzerland. The facility has particle accelerators, which undergo continuous upgrades. In these accelerators, particles are accelerated to high kinetic energies. These particles carry so much kinetic energy that when they are collided with each other, they break down into smaller particles. The smaller particles are so small that they cannot be detected with classical methods. For this purpose, a special type of semiconductor particle detectors have been developed for the experiments.

The detectors in Large Hadron Collider (LHC) are essentially reverse-biased, nano-sized, diodes. The diodes are usually biased in such way that they are fully depleted. When a particle passes through the detector, it causes a recombination of electron-hole pairs in the depletion zone. Due to the depletion, the electrons separate from the holes and travel to the anode, while the holes travel to the cathode, thereby generating an electrical current. This current can be detected, and when there are several detectors in a chamber, the trajectory and velocity of the particle can be defined.

Radiation causes lattice flaws in the silicon from which the detectors are fabricated. These defects affect both the sensitivity and the lifetime of the detector. At present, CERN is upgrading the LHC to the Super-LHC. The luminosity will multiply by ten times from the current luminosity to 10^{35} cm^{-2}s^{-1}, and the total fluence of fast hadrons will rise above 10^{16} cm^{-2}. Due to this increase in radiation, the lifetime of the detector will decrease. To investigate this problem, CERN has set up workshops whose purpose is to develop new methods for improving the radiation hardness of the detectors [1].

The purpose of this study is to identify and specify the effects of radiation induced defects on the leakage current of silicon based particle detectors. The goal is to create a model, and validate the capability of present program packages to simulate radiation induced defects.

The simulations employ a program package called Virtual Wafer Fab (VWF) made by Silvaco International inc. This simulates both manufacturing processes, and electrical properties of microelectronic devices.

2 Atoms

Atoms comprise a nucleus and electrons moving around it. The nucleus contains protons and neutrons, which are about 2000 times heavier than electrons; thus, nearly all the mass of an atom is concentrated in the nucleus, while most of the volume is occupied by the electrons. The properties of materials arise mostly from the electronic configuration. This, combined with the mass of the nucleus, can be used as an approximation in electronic structure calculations. Due to the heavy mass of the nucleus, its velocity is insignificant compared to the velocity of the electron, and the nucleus can, therefore, be approximated as stationary. This approximation is called Born-Oppenheimer approximation [2]. Protons carry a positive charge, while electrons are negatively charged, and neutrons are neutral particles. Elements are classified and characterized by the number of protons in their atomic nuclei. This number is called the *atomic number*, Z. The *atomic mass* A is the total mass of an atom. The number of neutrons N for given value of Z can vary. Such atoms are called isotopes.

An early model for atoms is due to Bohr. In it, the electrons circle around the nucleus in discrete orbits, and the energy states are quantized. This model is not exact, but has virtue in its simplicity. To describe the electrons more accurately, one needs to take into account the particle and wave-like characteristics of the electron. This is done by representing the electrons by wave-functions. This leads to probability distribution of the position of electrons. The radius which has the highest probability, is called the *Bohr radius*.

Quantum numbers are used to characterize electron states in wave mechanics. There are four quantum numbers for each electron, and they define the size, shape, spatial probability density and spin. The first quantum number is called *principal quantum number* n, which is expressed either as $n = 1, 2, 3, 4, \ldots$, or using the letters $\mathrm{K, L, M, N, O}, \ldots$, respectively. This number relates to the distance of the electron from the nucleus, or its position, and hence to the Bohr radius.

The second quantum number specifies the subshells which are denoted by $l = s, p, d$, and f. The second quantum number, called *azimuthal*, or *angular momentum* quantum number l, is restricted by the principal quantum number n such that $l \leq n$. Orbitals, corresponding to a quantum number l, have specific geometry, i.e. different probability density distributions. The third quantum number m_l defines the number of states for each subshell. The number of states in a subshell is $2l - 1$; hence, different subshells have different number of states. The fourth quantum number is spin. It can have only two

values: $-\frac{1}{2}$ and $+\frac{1}{2}$.

The states are filled according to the *Pauli exclusion principle*. This states that every state can hold up to two electrons, both with different spin. When combined with the quantum numbers, this gives the maximum number of electrons in each subshell s, p, d, and f, which are $2, 6, 10$ and 14, respectively. The electrons tend to adopt the lowest possible energy configuration, which is called the *ground state*. Electrons can be excited from their ground state by e.g. heat.

Electrons in the outermost filled shell are called valence electrons. These electrons are responsible for bonding, and most of the ordinary physical and chemical properties of matter. Electron configurations are called stable when the outermost shell is complete. The complete shell is defined as completely filled outermost s- and p-orbitals, i.e. eight electrons. Elements possessing a stable configuration are chemically inert; they are noble gases. Atoms possessing an incomplete shell can complete it either by becoming an ion or by sharing electrons with other atoms, i.e. bonding [3]

Most solid materials posses some form of crystal structure. In crystals, atoms adopt an ordered, periodic arrangement in space called a lattice. Its form is determined by the electronic structure of the atoms. If the electronic structure differs, then the atomic positions differ, and thus the electrical and physical properties of the materials differs. Forces of various types between atoms compel them to take specific places. There are repulsive and attractive forces between the nuclei and the electrons, and between nucleus and the neighbouring nucleus. Taking into account these different forces it is matter of geometry to fit as many atoms as possible to a small volume as possible.

Solids usually form ionic, covalent or metallic bonds. In an ionic bond an atom donates its outer shell electrons to another atom, and the atoms become ions. Ions with different charges attract each other due to Coulomb forces, which bind them together. This is balanced by a repulsion force arrising from the overlap of inner electron shells of the ions. At equilibrium, the total energy of the system is minimized. This determines the bond lengths. Even though the ions are electrically charged, the material itself remains neutral.

In covalent bonds atoms share their electrons, in pairs between them. The charge density is high between the atoms. The number of the bonds an atom can form depends on how far away the electronic configuration of the outermost shell is from the closed shell [2, 4].

In metallic bonds, the electrons of the outermost shell are separated from the host atoms and form a free electron gas. The binding energy of the metallic bonds arises from the attractive Coulomb force between the free electron gas and the charged ions.

2.1 Band Structure

Band structure arises from the electronic configuration of the individual atoms. When considering a lattice, the atoms are separated by specific distances in particular directions, which determines their interactions. When atoms are brought into close proximity, the atomic states split into several discrete states, as consequence of the Pauli exclusion principle. If there are N atoms, then the number of these split states for each band is $(2l - 1)N$, where l is the second quantum number, and each state can have two electrons with different spins. The energy difference between these states is very small and they are almost continuous. These states form electron energy bands, between which can be a band gap, or forbidden band, which is devoid of states, and that arises from the periodic potential of the lattice.

Bands can be fully filled, partially filled, or empty, which lead to four types of band structures. In the first, the *valence band* is partially filled, and the *conduction band* is empty. The *Fermi level* lies in the valence band. The Fermi energy is defined at 0 K temperature as the highest occupied energy state. This type of band structure occurs in e.g. copper and other metals. In the second, there is an overlap of the filled and empty bands. Metals, such as magnesium, exhibit this behaviour. The Fermi level in these materials lies in the overlapping part of the bands. The third type has a fully filled valence band, empty conduction band and a gap between them, so it is defined as an insulator. The fourth is essentially the same, but the difference is in the size of the gap. The gap is smaller in the fourth type than in the third, and thus the material is a semiconductor. In both of these types the Fermi level lies in the middle of the band gap.

The band gap itself can be either direct or indirect. Direct band gap means that the lowest energy of the conduction band occurs at the same wavevector as the highest energy of the valence band when the electron wave-functions are expressed as a Fourier expansion. A system with an indirect gap has its conduction band minimum and valence band maximum at different wavevectors. In this case, in order to conserve the crystal momentum, a lattice vibration or phonon is needed to excite an electron from the valence band to the conduction band. The optical properties of materials that posses a forbidden band depend

strongly on whether the band gap is direct or indirect.

2.2 Conductivity

For an electron to participate in the conductivity, it must have an energy higher than the Fermi energy. As such, the electron becomes a *free electron*. The excitation of the electron occurs due to some external energy, such as heat, photon absorbtion etc. When the electron is in a state above Fermi energy, an electric field can accelerate electrons. Another type of charge carrier is a *hole*. Holes are carriers mainly in insulators and semiconductors. For a hole to participate in conduction, it must have a lower energy than the Fermi energy. The total conductivity depends on the number of the free electrons and holes in a material.

In metals, the energy difference between the state above the Fermi energy and the top of the occupied valence band states is relatively small, and thus only a small amount of energy is required to excite an electron to the conduction band. Although the valence electrons in metallic bonds form a delocalized gas, they must still be excited to become free electrons.

For insulators and semiconductors, the valence band is fully filled and the conduction band is empty. In between there is a band gap. Therefore, there are no states available adjacent to the states at the top of the valence band, and more energy is required to excite an electron to the bottom of conduction band. The energy required depends on the size of the band gap. At higher temperature the system has more thermal energy and a smaller external energy is needed to excite the electron. If the band gap is wider, then the probability of an electron to have enough energy to be excited decreases, and fewer electrons are excited; hence, the conductivity decreases.

In semiconductors and insulators, a hole is created in the valence band when an electron is exited to the conduction band. Holes contribute to conduction in the valence band. When an electron is excited, it leaves an empty state in the valence band. An electron can fill the empty state resulting in an effective motion of the hole, thus producing a hole current.

2.2.1 Charge carrier mobility

Mobility is a parameter which describes the movement of the charge carriers in materials. An applied electric field accelerates free electron and holes. Due to their negative charge, electrons move in the opposite direction to the applied field, while holes move in the same direction as the field. Quantum mechanics states that the perfect lattice does not interact with the moving electrons, but the speed of the electrons is still limited. This is due to imperfections in the lattice, such as defects, and thermal vibrations. The electrons collide with defects and phonons, and their energy and direction change, thus generating resistance. This is called *scattering*. Even though the electrons scatter, on average they still move in the same direction, opposite to the electric field. The average rate of motion is called the *drift velocity*, and is defined as

$$v_d = \mu_e E, \tag{1}$$

where μ_e is the mobility of the electrons and E is the applied electric field. Mobility depends on both the material and temperature. The mobility of holes, μ_h is defined the same way, only the direction of the hole is opposite to the direction of the electron.

The conductivity σ of most materials is then defined as

$$\sigma = n|e|\mu_e, \tag{2}$$

where n is the number of charge carriers per unit volume and e is the charge of an electron.

2.3 Semiconductors

The conductivity of semiconductors differs somewhat from the conductivity of metals. When a semiconductor is pure, i.e. does not contain lattice imperfections or other types of defects, it is called an *intrinsic* semiconductor. In semiconductors, both electrons and holes contribute to the conductivity, and the conductivity can be described by

$$\sigma = \mu_e|e|n + \mu_h|e|p. \tag{3}$$

Since a hole is created when an electron is excited to the conduction band, the concentra-

tion of electrons and holes is the same

$$n = p = n_i, \tag{4}$$

where n and p are the number of electrons and holes per unit volume, respectively, and n_i is known as *intrinsic carrier concentration*. Combining equations (3) and (4) yields the result

$$\sigma = n|e|(\mu_e + \mu_h) = p|e|(\mu_e + \mu_h) = n_i|e|(\mu_e + \mu_h). \tag{5}$$

When the lattice is imperfect and includes defects, the situation is different and is called an *extrinsic* semiconductor. Essentially, all manufactured semiconductors are extrinsic. Defects are inevitably present; however, in this case the defects are intentional, for purpose of modifying the properties in a specific manner. This process is called *doping*. The concentration of impurities required to make an extrinsic semiconductor is extremely low, being only the order of 10^{-7} at%.

2.3.1 *N*-type extrinsic semiconductor

N-type semiconductors form when impurity atoms possessing more electrons in their outer shell that the atoms of the host material, replace host atoms in its lattice. When e.g. silicon (Si, group IV) is doped with phosphorous (P, group V) only four of the five outermost electrons of the P are bound to bonds, and one is left over. This electron lies in a state in the band gap, near the bottom of the conduction band, and therefore need only a small amount of energy to be excited to the conduction band. This event will not create a hole, so the concentration of electrons increases with respect to the concentration of holes. The atom donates an electron and thus is called a *donor*. The state which it creates to the band gap is called a *donor state*. The donor atom raises the Fermi energy higher in the band gap, nearer to the donor level. In addition, the intrinsic excitations occur, however the number of electrons dominate, thus are called *majority charge carriers*, while the holes are *minority charge carriers*. Since $n \gg p$, the conductivity becomes

$$\sigma \cong n|e|\mu_e. \tag{6}$$

2.3.2 *P*-type extrinsic semiconductor

In p-type extrinsic semiconductors, impurity atoms possessing fewer electrons in their outer shell than the atoms of the host material, replace host atoms in lattice. Therefore, at least one of the bonding states is left empty. This empty state can be filled by an electron from a neighbouring atom, with a small energy. In this way the hole moves in the same direction as an applied external field. In terms of band model, the acceptor atom creates a state in the band gap, near the top of the valence band. The electron is promoted to this state by thermal excitation and leaves a hole behind. Therefore, $p \gg n$, and the holes are majority charge carriers, while the electrons are minority charge carriers. Thus, the conductivity can be written as

$$\sigma \cong p|e|\mu_h. \tag{7}$$

The state which acceptor atom creates in the band gap is called an *acceptor state*.

2.4 Defects

In every material, there are lattice imperfections. These imperfections are called *defects*. The defects are classified as point defects, dislocations, plane and bulk defects. They are characterized by their geometry. The two most important defects are point defects and dislocations. Bulk defects are important in the field of radiation induced defects, and are mostly vacancies or impurity atom clusters. Defects affect the electrical and mechanical properties of materials.

2.4.1 Point defects

As the name *point defects* suggests, these are point-like entities. They consist of interstitial atoms, substitutional atoms, or vacancies. An interstitial atom can be the same kind of an atom as the lattice is, or it can be of different type. The term interstitial means that the atom is at a non-lattice site, in the interstices or spaces between the lattice atoms.

Substitutional defects are impurity atoms which replace a host atom at a lattice site. An impurity atom has a notional radius. When this differs from that of the host, local distortion of the lattice occurs. This leads to a change in the average lattice parameter in

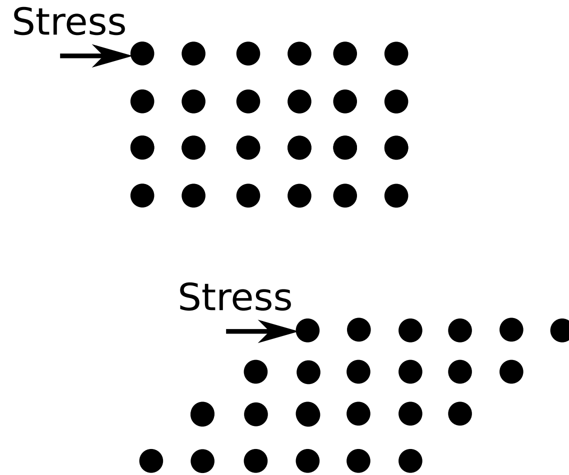

Figure 1: Plastic deformation of a perfect crystal. After Ref. [5].

proportional of the effective radius of the impurity atom and its concentration.

A lattice vacancy is essentially a substitutional defect; it is an unoccupied lattice site. Usually this causes the surrounding lattice to relax inwards, distorting the lattice. The density of the crystal then depends the magnitude of this distortion, and vacancy concentration.

When a vacancy is paired with a interstitial atom, it is called a *Frenkel pair* or *Frenkel defect*. In addition, in a diatomic ionic crystal, when there is an even number of both type of vacancies, i.e. from positive and negative ion sites, this state is called a *Schottky defect*.

Vacancy related defects are often refered as centres. In diatomic ionic crystals, two neighbouring negative ion vacancies are called *M*-centre. In silicon, the *E*-centre consists of a vacancy next to a substitutional group V atom, such as phosphorous. *E*-centres play an important role in the doping of silicon [5].

2.4.2 Dislocations

Dislocations are topological, linear defects, and they are nearly always present in a real specimen. Their existence was invoked to explain why the yield stress of crystals—at which they undergo permanent, plastic deformation—is so much smaller than the shear modulus. In a perfect crystal, the critical shear stress required permanently to deform it, requires that all atoms in one crystal plane slip over the neighbouring plane (see figure 1). Since this would involve simultaneously breaking all the atomic bonds between the two

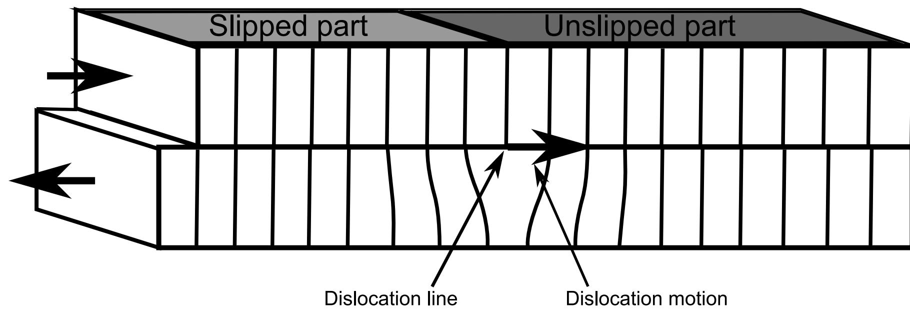

Figure 2: Schematic illustration of slip in a crystal via the motion of an edge dislocation. After Ref. [5].

planes undergoing slip, the strength of crystals should be very much greater than is observed in reality. Dislocations allow slip occur by the propagation of a topological kink in the crystal along a line atoms, such that its motion only involves one atom at a time, thereby lowering the activation energy of the process.

An edge dislocation can be imagined by introducing one half plane of atoms in between two planes of atoms (see figure 2). Thus, the atoms everywhere else than in the vincinity of the dislocation line, are in a perfect crystaline order. In a screw dislocation one end of the atom planes remains undisplaced, while part of the other end is shifted in the direction of a lattice vector (see figure 3).

Dislocations are described in terms of a Burgers vector. A closed path taken in a perfect lattice (e.g. five planes down, six to the right, five upwards, and six to the left) involves no net displacement to complete it. If a dislocation is present, then an additional component must be added to return to the origin. This amount is defined as the Burgers vector [5].

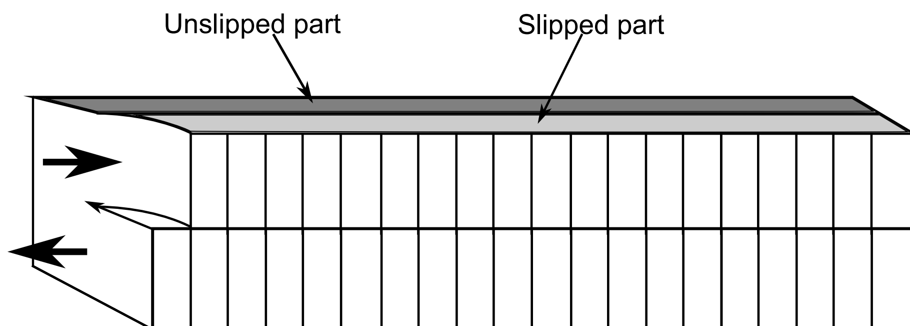

Figure 3: Schematic illustration of slip in a crystal via the motion of an screw dislocation. After Ref. [5].

Dislocations can interact with one another, in a manner so that they become locked together. In these situations, such as occurs during the cold working of metals, the material becomes stronger, owing to the overlap of dislocation strain fields.

2.4.3 Plane defects

Plane defects, or surface imperfections, often take form of stacking faults. For example, in a lattice that consists of two layers of close-packed, spherical atoms, where the second layer resides over the hollow sites of the first (i.e. in its interstices), the structure posses sixfold symmetry. Using labels A and B to represent each of the two layers, these are then repeated in space . . . ABABABABAB . . . . The resulting lattice is described as being hexagonal close-packed (hcp).

Starting with the original two layers, a third layer labelled C, can be located such that its atoms are *not* above those in the first A. The next layer, however, is aligned with the first layer, now making the sequence . . . ABCABCABC . . . when repeated. This lattice has cubic symmetry, defined as face-centered cubic (fcc).

Stacking faults can occur when one layer is out of sequence, and the following ones then come in reverse order, . . . ABCABCBACBA . . . . On each side of the boundary, the crystal is otherwise perfect. A plane defect can also take the form of a junction, where two single crystals with different crystal orientation intersect. In this case a grain boundary is formed. Several different types of grain boundaries can be found and they are present in most real crystal [5].

Stacking faults are often associated with dislocations. In certain circumstances, the local strain in the vicinity of a dislocation can be relieved by introducing a stacking fault between two *partial* dislocations, thereby lowering the total energy of the system. This phenomenon is known as *dissociation* of a dislocation.

3 Semiconductor particle detectors

At present, the detectors installed at the LHC consist of microstrip detectors and pixel detectors. Microstrip detectors are situated closest to the beam. The outer detector is

constructed using pixel detectors. The main idea behind the semiconductor position-sensitive particle detectors is simple. The chamber is filled with small semiconductor detectors, which yield a signal when a particle travels through the chamber. When the number of the detectors is large, the position and velocity of the particle can be traced by tracking the trajectory of the signal, and thus the particle and its properties can be identified.

Developement of detectors is an ongoing process, and it covers areas from materials engineering to structural design. Current detectors are fabricated from silicon; however, several possibilities for new materials have been suggested. Also, improvement in the silicon detectors are being investigated. New structures have been introduced as well, such as 3D detectors [6, 7, 8], and current injected detectors [9] (CID), which are a completely new design.

3.1 P-n junction

When a junction is manufactured in such a way that one region is doped with donor atoms and the other with acceptor atoms, it forms a *p-n junction*. This type of junction is the key structure in present integrated circuit (IC) technology, and has made, e.g. microcomputers possible. Semiconductor particle detectors are also based on this type of junction, or more precisely, on the depletion of this junction.

Assume the junction is located at $x = 0$. In addition, let $N_d(x)$ be the donor density and $N_a(x)$ the acceptor density as a function of position. The distribution of the doping atoms is called the *doping profile*. Next, assume that the doping profile is nonuniform in the vicinity of $x = 0$. The nonuniformity in doping affects the conduction band electron density, $n_c(x)$, and the valence band hole density, $p_v(x)$, distributions, which in turn affect the potential across the junction, $\phi(x)$. The region in which the charge carrier densities are nonuniform is called the *depletion zone* or *space charge region*. In this region the charge carrier concentration is small. This happens due to the fact that electrons from the n-region diffuse to the p-region, while holes from the p-region diffuse to the n-region, thereby creating an intrinsic region in the junction. An intrinsic semiconductor itself is usually an insulator, so there is no major current through the depletion zone at equilibrium.

If the transition is assumed to be sharp, then

$$N_d(x) = \begin{cases} N_d, & x > 0 \\ 0, & x < 0 \end{cases}$$
$$N_a(x) = \begin{cases} 0, & x > 0 \\ N_a, & x < 0. \end{cases} \tag{8}$$

The generalized charge carrier densities can be described as

$$n_c(x) = N_c(T) \exp\left\{-\tfrac{[\varepsilon_c - e\phi(x) - \mu]}{k_\mathrm{B}T}\right\}$$
$$p_v(x) = P_v(T) \exp\left\{-\tfrac{[\mu - \varepsilon_v + e\phi(x)]}{k_\mathrm{B}T}\right\}, \tag{9}$$

where μ is the chemical potential of the material and $\varepsilon_{c,v}$ are the conduction band and valence band edges, respectively. $\phi(x)$ is the electrostatic potential caused by the junction.

Far away from the junction, the density of the conduction band electrons is nearly equal to N_d on the n-side of the junction, and the density of holes, N_a, on the p-side. Therefore,

$$N_d = n_c(\infty) = N_c(T) \exp\left\{-\tfrac{[\varepsilon_c - e\phi(\infty) - \mu]}{k_\mathrm{B}T}\right\}$$
$$N_a = p_v(-\infty) = P_v(T) \exp\left\{-\tfrac{[\mu - \varepsilon_v + e\phi(-\infty)]}{k_\mathrm{B}T}\right\}. \tag{10}$$

In thermal equilibrium μ does not depend on the position; hence, the total potential drop across the junction is

$$e\phi(\infty) - \phi(-\infty) = \varepsilon_c - \varepsilon_v + k_\mathrm{B}T \ln\left[\frac{N_d N_a}{N_c P_v}\right]. \tag{11}$$

Consequently,

$$e\Delta\phi = E_g + k_\mathrm{B}T \ln\left[\frac{N_d N_a}{N_c P_v}\right]. \tag{12}$$

Equation (12) gives the boundary conditions for the differential equation of $\phi(x)$, which is essentially Poisson's equation,

$$-\Delta^2\phi = -\frac{\partial^2\phi}{\partial x^2} = \frac{4\pi\rho(x)}{\epsilon}, \tag{13}$$

where ϵ is the static dielectric constant of the material and $\rho(x)$ is the charge distribution. The charge density due to impurities and carriers is

$$\rho(x) = e[N_d(x) - N_a(x) - n_c(x) + p_v(x)]. \tag{14}$$

The result obtained by substituting the carrier (8) and impurity densities (9) into equation (14), is then substituted to the Poisson's equation (13). There is no analytical solution to this; hence, it is necessary to either use approximations, or numerical methods.

By using the approximation that the total change of potential $e\phi$ is order of $E_g \gg k_\mathrm{B}T$, and combining it with equations (9) and (10) gives

$$\begin{aligned} n_c(x) &= N_d \exp\left\{-e\frac{[\phi(\infty)-\phi(x)]}{k_\mathrm{B}T}\right\} \\ p_v(x) &= N_a \exp\left\{-e\frac{[\phi(x)-\phi(-\infty)]}{k_\mathrm{B}T}\right\}. \end{aligned} \tag{15}$$

The change in potential, $\Delta\phi$, occurs in the region $-d_p \leq x \leq d_n$, and the potential has an asymptotic value everywhere else. The quantities d_p and d_n are the lengths of the p- and n-type regions, respectively. The densities of charge carriers are, therefore, $n_c = N_d$ in the n-region, and $p_v = N_a$ in the p-region, with $\rho = 0$. Inside the region, $n_c \ll N_d$ and $p_v \ll N_a$, since the potential $e\phi$ differs several $k_\mathrm{B}T$ from its asymptotic value. From this, to a good approximation, $\rho(x) = e[N_d(x) - N_a(x)]$ in the space charge region, and thus the points $x = -d_p$ and $x = d_n$ are the boundaries of the depletion zone.

Consequently, using equation (8), Poisson's equation becomes

$$\phi''(x) = \begin{cases} 0, & x > d_n \\ -\frac{4\pi e N_d}{\epsilon}, & d_n > x > 0 \\ \frac{4\pi e N_a}{\epsilon}, & 0 > x > -d_p \\ 0, & -d_p > x \end{cases}. \tag{16}$$

Integration yields the result

$$\phi(x) = \begin{cases} \phi(\infty), & x > d_n \\ \phi(\infty) - \left(\frac{2\pi e N_d}{\epsilon}\right)(x - d_n)^2, & d_n > x > 0 \\ \phi(-\infty) + \left(\frac{2\pi e N_a}{\epsilon}\right)(x + d_p)^2, & 0 > x > -d_p \\ \phi(-\infty), & x < -d_p \end{cases}. \tag{17}$$

The boundaries of the depletion zone, $x = -d_p$ and $x = d_n$, and $x = 0$ create two new equations which determine the lengths, d_n and d_p. In addition, $\phi'(x)$ must be continuous at $x = 0$. This gives

$$N_a d_p = N_d d_n, \tag{18}$$

which implies that the total positive charge of the p-region is equal to the total negative charge of the n-region. Now, $\phi(x)$ must be continuous at $x = 0$, and this requires that

$$\left(\frac{2\pi e}{\epsilon}\right)(N_d d_n^2 + N_a d_p^2) = \phi(\infty) - \phi(-\infty) = \Delta\phi. \tag{19}$$

Equation (19) together with equation (18) determine the lengths of the n- and p-regions,

$$\begin{aligned} d_n &= \left(\frac{\epsilon\Delta\phi N_a}{2\pi e(N_a+N_d)N_d}\right)^{\frac{1}{2}} \\ d_p &= \left(\frac{\epsilon\Delta\phi N_d}{2\pi e(N_a+N_d)N_a}\right)^{\frac{1}{2}}. \end{aligned} \tag{20}$$

The depletion zone forms even at equilibrium, generating what is known as the *built in potential*, V_0, which is the potential caused by the p-n junction.

The depletion zone can be modified by doping. Increasing doping concentration on one side widens the length of the depletion zone on the other. External voltage also modifies the junction. When a forward bias voltage is applied to the junction, the depletion zone narrows, and the current is able to pass the junction. Reverse bias increases the width of the depletion zone. This is the desired behaviour for particle detectors [5, 10].

3.2 Operation principle

The underlying operational principle for the particle detectors at CERN relies upon the depletion of the space charge region in the p-n junction and collecting charge carriers. At the heart of the planar detectors is a P-I-N (p-type, intrinsic, n-type) diode, which is fully depleted. High-resistivity n-type silicon in the central region is depleted by applying a negative potential to the p-type contact and a positive potential to the n-type contact. When a particle enters the depletion zone of the diode, it creates electron-hole pairs along its path. Electrons and holes are then collected at the n- and p-type contacts, respectively.

The collection efficiency is called *charge collection efficiency* (CCE) and is an important

parameter for the detector. The collected charge Q_S is proportional to the energy lost by the incident radiation in the diode:

$$Q_S = \frac{E}{E_p} e, \quad (21)$$

where E_p is the energy required to form a electron-hole pair. In the case of silicon E_p = 3.6 eV.

The rms statistical fluctuation of the charge is

$$\Delta Q_S = \sqrt{F \frac{E}{E_p}} e, \quad (22)$$

where F is the so called *Fano factor*, which describes the deviation from normal Poisson statistics. In the case of silicon, this factor is $F \sim 0.1$ [10].

3.3 Leakage current

Leakage current occurs even in the depletion region of the diode. It is mostly harmful; therefore, it should be minimized. The leakage current comprises two different volume components, and a surface contribution.

The first volume leakage arises from minority charge carriers. The *p*- and *n*-regions repel majority carriers from the junction, but attract the minority carriers, which subsequently diffuse and cause a small current. This minority carrier current is so small that it can be neglected.

The other volume leakage arises from thermal generation of electron-hole pairs within the depletion zone. This current is affected by the volume of the space charge region, material and temperature. This current is sufficiently small in silicon, but still it causes the majority of the leakage current. The leakage current can described using

$$I_g = \frac{n_i}{2\tau} q\Lambda, \quad (23)$$

where n_i is the intrinsic carrier concentration, τ is the generation lifetime and Λ is the volume of the space charge region [10].

Surface leakage occurs near the edges of the junction where the gradient of the voltage is high. The surface leakage current depends on the design of the detector, encapsulation, environment and contamination of the detector surface. Surface leakage current can be decreased by employing structures such as guard rings. Present designs and fabrication processes have essentially eliminated the problem; therefore, surface leakage can be neglected.

The leakage current decreases the sensitivity of the detector, but also affects the bias voltage required to deplete the diode. The bias voltages of the detectors are usually applied through a high-value series resistor. Thus, the increase in the leakage current causes the voltage across the detector to decrease. Hence, the bias voltage needs to be increased.

Measurements of the leakage current provide a practical way to monitor the detectors. The leakage current should be stable and increase a by small amount with an increase in the bias voltage; however, any major changes in the leakage current usually signals the presence of an abnormality in the detector, e.g. nearing the breakdown voltage, or some unspecified malfuction. Long term leakage current monitoring reveals accumulated radiation damage in the detectors [11].

3.4 Strip Detectors

The *Compact Muon Solenoid* (CMS) at the LHC consists of silicon microstrip detectors and pixel detectors. See Ref. [12] for details of its design. The microstrip detectors are single sided 'p^+ on n' diodes with a metal over-hang to achieve as high as possible breakdown voltage [13]. In order to make strip-shaped diodes, the p^+ implantations are done on the front. The aluminium readout strips are capacitively coupled to p^+ implantated strips. The aluminium strips are 15% wider than the p^+ strips. The bias resistors of the strips are polysilicon resistors. The design of the strips for the CMS uses three ways to maximize the radiation hardness.

Firstly, the devices are fabricated with ⟨100⟩-oriented silicon, instead of the more usual ⟨111⟩ orientation. This reduces the number of surface dangling bonds, resulting in lower interstrip capacitance by suppression of surface damage.

The metal over-hang over the p^+ strip increases the stability of the detector at higher bias voltages up to 500 V. The over-hang produces an improved field configuration. High

field gradients near the edges of the metal over-hang are avoided by extending the plates beyond the implantation.

Use of low resistivity bulk silicon retards the inversion point of the diodes, and thus gives a lower depletion voltage after irradiation.

The back of the sensor is n^+ doped to create an ohmic contact between the bulk and metal contact. This also acts as a barrier for the minority charge carriers from the space charge region (SCR) to the contact, and for the majority charge carriers from the contact to the SCR, resulting in a very low leakage current. On the junction side, the n^+ area lies along the edges preventing the SCR from reaching the cutting edge. In addition, this protects the active area from injection of charges from the heavily damaged edge region.

Two p^+ type guard rings surround the active region. The outer ring is to prevent the leakage current from the edge area to the internal ring. The internal ring is used to bias the strip. Together with the over-hang, the guard rings provide a multi-guard structure which smooths the electric field.

3.5 Pixel detectors

Part of the CMS consists of pixel detectors. The pixel detectors are '*n*-on-*n*' type detectors, with dimensions $100 \times 150\ \mu\text{m}^2$ and 285 μm thick. The base material for these pixel detectors is float zone (FZ) silicon which is diffusion oxygenated to give better post radiation behaviour. The crystal orientation of the silicon is $\langle 111 \rangle$. The biasing grid and inter-pixel isolation is done by a moderate *p*-spray technique [14]. The minimum size of the pixels is defined by the area required by the readout strips.

A pixel detector consists of high dose *n*-type implant in a highly resistive and lightly doped *n*-substrate. The back of each pixel is *p*-doped, thereby forming a *p*-*n* junction. The SCR must not reach the edge of the detector; hence, a double-sided process is required. In addition, attention must be paid to the electron accumaltion layer, which causes a reduction in the SCR, making the effective thickness of the device smaller.

n-on-*n* detectors are more expensive than the standard *p*-on-*n* detectors. The advantages of the *n*-on-*n* detectors are good signal in moderate bias voltage after irradiation; high electron mobility, and thus better spatial resolution; and owing to the double-sided pro-

cess, a guard ring scheme can be implanted, allowing the entire sensor edges to be electrically grounded [15].

3.6 Radiation induced damage

While passing through the detector, radiation induces defects to the material. Ionizing energy transfer that goes only into creating electron-hole pairs causes no irreversible damage to the material. Lightly ionizing radiation, such as beta particles and gamma rays, cause minor damage. Major damage arises from heavy charged particles. Radiation induced damage causes the leakage current to increase, and hence degrades the energy resolution. Furthermore, the atomic displacement damage in the detector bulk increases the effective doping concentration (N_{eff}), and consequently the operational voltage must be raised to compensate. It also affects the effective doping concentration of the detector [16]. The damage produced depends strongly on the nature of the radiation. Radiation damage can be divided into tow categories: bulk and surface defects.

Bulk damage consists of Frenkel defects and defect clusters, and is vacancy related. Frenkel defects form as a result of the displacement of atoms from their lattice sites. These atoms form a pair with an interstitial atom and can act as a trap for charge carriers. Clusters form along the track of the radiation when the primary knock-on atom (PKA) carries sufficient energy. Radiation with relatively small energy causes point defects, while heavy particles with high energy cause clusters. Bulk defects reduce carrier lifetimes, reduce CCE and cause degradation of the energy resolution.

The surface effects are more directly responsible for the increase of the leakage current, and also contribute to a loss of detector resolution owing to fluctuations in the leakage current. The surface effects are closely related to the ionization created within the passivation oxide of the detector and its trapping at the interface. The direction of incidence of the charged particle and electron radiation affect the formation of surface damage. Irradiation of the front surface of a fully depleted detector produces more damage than irradiation of the back contact [11].

Radiation induced defects have been studied for over 50 years, yet many open questions remain. For example Watkins and Corbett [17, 18, 19] were among the first ones to study vacancies and divacancies in Si using electron paramagnetic resonance (EPR).

3.6.1 Vacancies

The lattice vacancy is one of the most fundamental defects in any crystal. Its atomic and electronic structure in silicon has been described in detail by Watkins [20]. A vacancy is formed when radiation knocks an atom from its lattice site. When the energy of the radiation is low, the recoiled nucleus obtains less kinetic energy; hence, no further displacements occur. The displaced nucleus diffuses away from the vacancy site and becomes an interstitial atom, which is another fundamental defect.

The vacancy in silicon V_{Si} has five different charge states (V^{+2}, V^{+}, V^{0}, V^{-}, V^{-2}). It has the distinction of being one of the first defects where the negative-U effect was observed [21]. In the negative-U effect, the ordering of the states is reversed, which here means that it is energetically beneficial to trap two electrons instead of one. The negative-U effect is a direct result of a large Jahn-Teller distortion, occuring when the energy gained exceeds the Coulomb repulsion energy.

The Jahn-Teller distortion for silicon has mainly tetragonal character, which gives D_{2d} symmetry for the defect, and can occur in two opposite ways. The six Si-Si distances around the vacancy are divided into two sets of four and two equivalent Si-Si lengths. One type distorts pairwise the two equivalent Si-Si lengths to be longer than the fourfold equivalent set. The other type is the other way around. When the system contains sufficient electrons to occupy the e state, the symmetry is lowered to C_{2v}, where the twofold equivalent Si-Si lengths in the D_{2v} becomes unequal [22].

The different charge states have different lattice relaxations, and therefore diffusion of the defect and interactions with other charged defects depend on the charge state of the vacancy.

Vacancies, are highly diffusive. The diffusion of a vacancy is long-ranged, and the vacancies tend to pair up with other defects such as interstitial oxygen, substitutional impurities, and other vacancies. It has also been identified that the single vacancy can contain H_2 molecules [23]. Pintilie *et al.* [24] suggest that the formation of V_2O occurs via oxygen trapping a vacancy, followed by the VO complex trapping another vacancy.

At elevated temperatures all charge states exist as the vacancies trap and emit thermally generated electrons and holes. This complicates the migration process. In general, the contribution to the migration comes from the vacancy formation energy, while thermally

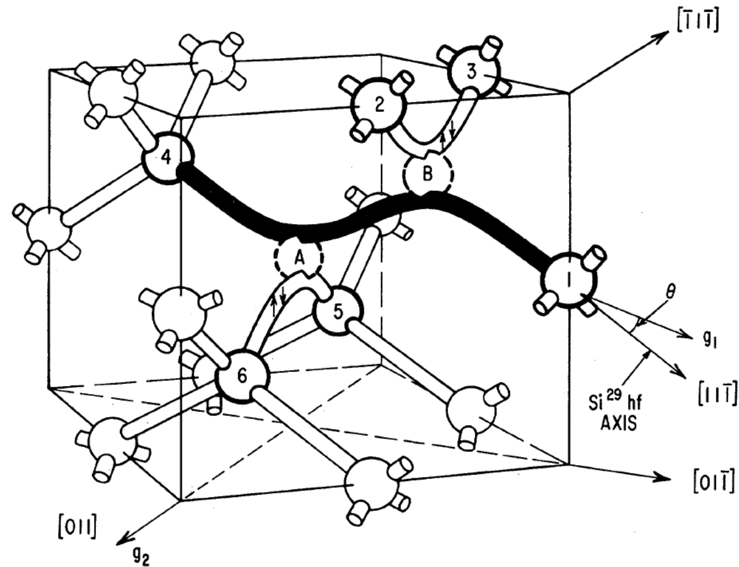

Figure 4: Strucuture of divacancy, showing the atoms and bonds between them. The dashed circles are the missing atoms[18].

activated diffusion is small.

With higher energy radiation, the recoiling nuclei carry higher kinetic energy, and hence the nuclei displace other atoms in a highly localised region. This causes clustering of vacancies, which results in V_n complexes.

Watkins and Corbett identified the divacancy in silicon in early 1960's [19]. They state that the creation of a divacancy does not require migration of vacancies. The divacancy forms from two nearest-neighbouring vacancies. This can occur when high energy radiation knocks an atom from its lattice site, and the recoiling atom has sufficient kinetic energy to knock the nearest-neighbouring atom from its site as well. In addition, both atoms must have sufficient kinetic energy after collision to become interstitial atoms. It is also known that the formation of a divacancy can occur via diffusion of vacancies [20].

In figure 4, the electrons on the atoms labelled 2 and 3 pair in molecular bonds, as do atoms 5 and 6. A single unpaired electron resides in the extended orbital between the atoms labelled 1 and 4, and thus the divacancy is a singly ionized donor. When a third electron is added, it occupies the antibonding orbital between the atoms 1 and 4, putting the divacancy into a singly ionized acceptor state.

The perfect divacancy has a D_{3d} symmetry and two doubly degenerate deep levels, e_u and

e_g, allowing four different charge states. The e_g level is empty and the e_u level is occupied by one, two, or three electrons in V_2^+, V_2^0, or V_2^-, respectively. This leads to distortion of the lattice, thereby lowering the electronic energy. Lowering the symmetry to C_{2h}, splits both e levels to a and b levels. The Jahn-Teller distortion is so large that the a_g level drops below the a_u level, consequently producing a negative-U effect. The V_2^{-2} state undergoes a only breathing mode displacement [25, 26].

The four different charge states of the divacancy mean it has three different energy levels. These are $E_v + 0.20$ $(+/0)$, $E_c - 0.41$ $(0/-)$, $E_c - 0.23$ $(-/-2)$ [16]. Divacancies, like vacancies, can diffuse easily.

The divacancy is a stable defect well above room temperature. Monakhov *et al.* [27] state that the annealing of divacancies occurs via a first-order mechanism. Diffusion and interaction with impurity atoms occurs in Czochralski (Cz) silicon, while in float zone (FZ) Si, as suggested by Watkins and Corbett [19], it occurs by dissociation with a higher energy. In contrast to Pintilie *et al.* [24], Monakhov *et al.* suggest that the annealing of divacancies leads to a formation of new centre with two charge states close to the energy of the V_2 $(-/0)$ and V_2 $(-/-2)$ levels. The capture cross section of the singly negative state is larger, while the doubly negative is similar, with respect to the corresponding states of the divacancy. Monakhov *et al.* suggest this is a divacancy-oxygen complex (V_2O).

Vacancies can cluster to even more complex defects V_n. These defects are poorly known due to their numerous, varied formation possibilities and structural arrangements. For example, Makhov and Lewis have used *density functional theory* (DFT) to investigate vacancy clustering [28].

The trivacancy has been suggested to be responsible for certain peaks in DLTS spectra by Ahmed *et al.* [29], and recently, Bleka *et al.* has suggested possibility of a {110}-planar tetravacancy chain [30].

The most stable configuration of V_n defects has been calculated to be the ring-hexavacancy V_6 by Hastings and Estreicher *et al.* [31, 32]. They have calculated that the formation of hexavacancies occurs most likely via stacking of monovacancies, combined with rapid collapse to the ring-hexavacancy formation from any other hexavacancy configuration. The ring-hexavacancy has trigonal symmetry, and is nearly planar. This supports the experiments performed by Chadi and Chang [33], which recognised the stability of V_6 already in 1988. The V_6 defect is stable, due to the almost perfect crystal reconstruction around it; the reconstruction involves 14 host atoms, and hence the silicon atoms adjacent

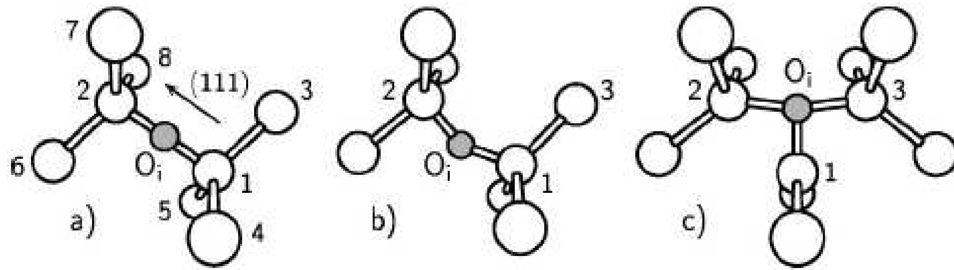

Figure 5: The configurations for interstitial oxygen, a) D_{3d} symmetry, b) C_{1h} symmetry and c) Y-lid configuration. The grey atoms are oxygen [35].

to the hexavacancy are nearly perfectly fourfold coordinated.

The hexavacancy does not posses—unlike other vacancy complexes—any deep levels in the band gap, and therefore the hexavacancy is believed to be electrically inactive. Due to its large size, it is considered to be a gettering centre for impurity atoms.

3.6.2 Vacancy-oxygen complexes

Oxygen is a common impurity atom in silicon, and it is an efficient trap for vacancies. This results in the formation of different types of vacancy-oxygen complexes $V_n\mathrm{O}_m$. Hence, vacancy-oxygen complexes are among the main defects in irradiated silicon, yet they are not fully understood.

In silicon, an oxygen atom locates itself near the interstitial bond-centre site with two equal Si-O bonds. The symmetry can, in principle, be C_1, C_{1h}, C_2 or D_{3d}, depending on the position of the oxygen with respect to the back-bonded silicon atoms (see figure 5). Oxygen diffuses in silicon by hopping to neighbouring bond-centres, with effective symmetry of D_{3d}, and diffuses easily [34, 35].

The possible structures of oxygen dimers in silicon are presented in figure 6, where the staggered configuration is the most stable configuration. The oxygen dimer can diffuse even faster than the isolated oxygen.

The VO, or A-centre, is one of the most common defects in irradiated silicon at room temperature. In addition it is the dominant defect in Cz-Si after MeV electron irradiation [36].

The VO defect has two different charge states (VO^0 and VO^-), and VO is mobile. It is believed to form via a diffusing vacancy, being trapped by interstitial oxygen. The A-centre has C_{2v} symmetry, where the oxygen atom is attached to the dangling bonds of neighbouring silicon atoms. The structure of VO can be seen in figure 7 a).

Due to the fact that the VO complex is highly diffusive, it can encounter an interstitial oxygen O_i, or another VO, and hence, form VO_2 or V_2O_2 defects, respectively.

The V_2O defect is proven to be harmful in terms of leakage current for the detectors. It has been observed to have a neutral charge state at 0.50 ± 0.05 eV and a deep acceptor level at 0.545 eV below the conduction band. The measured capture cross sections for the acceptor state are $\sigma_n = (1.7 \pm 0.2) \times 10^{-15}$ cm^2 and $\sigma_p = (9 \pm 1) \times 10^{-14}$ cm^2 for electrons and holes, respectively. The observed acceptor level of the divacancy-oxygen contributes to both leakage current and effective doping concentration [24]. The structure of V_2O is illustrated in figure 7 c).

The V_2O defect can form via a second-order process, $VO + V \rightarrow V_2O$, or theoretically via $V_2 + O \rightarrow V_2O$ [34]. Therefore, the possibility of introducing oxygen dimers into silicon, and thus suppressing the formation of V_2O defects has been studied. In the case of oxygen dimers, a more probable defect would be VO_2, which is not electrically active. In addition, formation of V_2O_2 would still be possible; the divacancy-dioxygen defect is at present considered to be perhaps less harmful than divacancy-oxygen [37, 38].

The VO_2 defect possesses D_{2d} symmetry, where both of the oxygen atoms are in a bridge between the silicon atoms, next to the vacancy (see figure 7 b)). This defect is believed to be electrically inactive. V_2O_2 has not yet been studied much, but it is presumed to be less

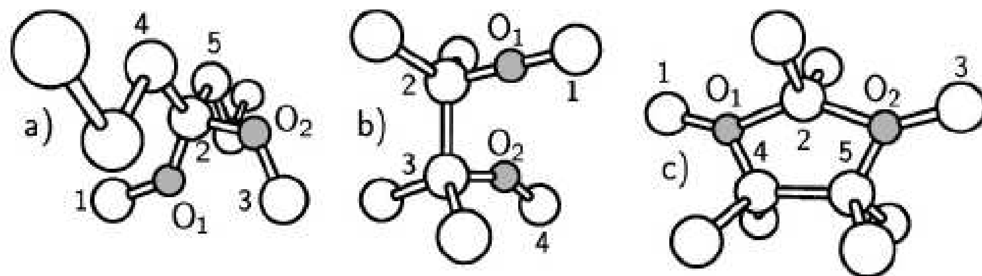

Figure 6: The configurations of oxygen dimers in silicon, a) staggered, b) skewed, and double-Y lid. Oxygen atoms are coloured grey [35].

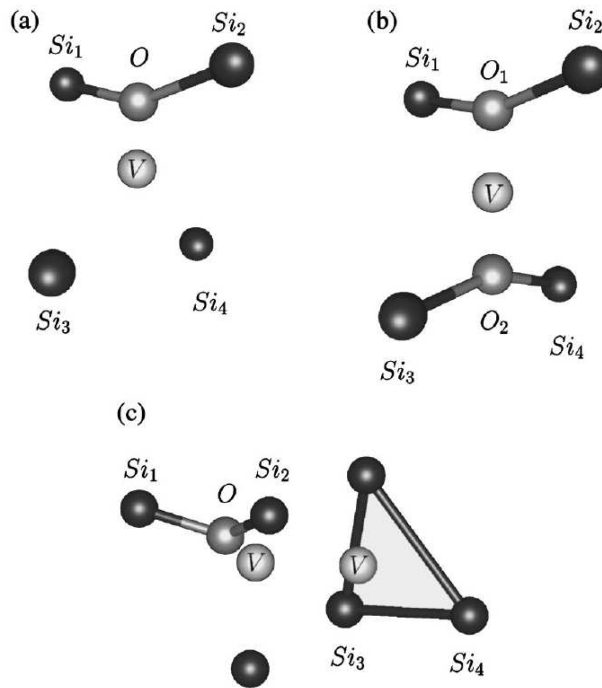

Figure 7: Calculated configurations of a) VO, b) VO_2 and c) V_2O. The dark grey atoms are silicon, lighter grey are oxygen and V stands for vacancy [34].

harmful than the V_2O [37].

It has been suggested that hydrogen can passivate vacancy type defects. Hydrogen tends to saturate the dangling bonds of silicon atoms surrounding a vacancy, and it accelerates the diffusion of oxygen atoms; thus, it promotes the formation of oxygen dimers. In addition, H promotes the annealing of VO and V_2 defects, and accelerates the formation of shallow donors [37].

Oxygen atoms are believed to contribute to the formation of thermal donors (TD) [39]. The oxygen related thermal donors are so called bistable donors (BD) [40]. Thermal donors provide a possible means to control the type inversion, and tailor the background resistivity of the material. This is due to the fact that the formation of shallow donors, created by TDs, compensates the deep acceptor levels. It is also known that increased radiation increases the introduction rate of TDs, and hence permits overcompensation of the change in the effective doping.

3.6.3 E-centers, Carbon and minority defects

Carbon is a highly effective trap for interstitial silicon and impurity atoms. A carbon atom is converted from the substitutional site to the interstitial via reaction $C_s + Si_i \rightarrow Si_s + C_i$. The interstitial carbon is highly diffusive [29]. Therefore, an interstitial silicon atom is bound to encouter an interstitial oxygen or substitutional carbon atom and form a more stable defect, C_iO_i, or C_sC_i, respectively [41]. Due to the higher concentration of oxygen, C_iO_i is a more common defect [42]. As an interstitial, the carbon ends up in split-$\langle 100 \rangle$ configuration sharing a lattice site with a silicon atom [20].

Boron has properties similar to carbon in silicon. It is a fast diffuser, forms similar defects, and traps other impurities, but is then re-released at higher temperatures. The difference is that the boron atom resides exclusively at an interstitial site, slightly off the centre of a Si-Si bond. It also exhibits negative-U behaviour [20]. Energy levels of B_sV have been measured by Londos [43] to be E_v + 0.31 eV and E_v + 0.38 eV, together with a bistable configuration by Zangenberg *et al.*[44] at E_v + 0.11 eV.

The most dominant defect induced by electron irradiation in P doped float zone silicon is the E-centre. The E-centre consists of a vacancy next to a substitutional group-V atom. It has an acceptor level at $E_c - 0.45$ eV, $E_c - 0.47$ eV, and $E_c - 0.44$ eV, for P, As, and Sb, respectively. It also has recently been suggested by Nylandsted-Larsen *et al.* [45] to have a donor level at about E_v + 0.2 eV.

In case of PV, there are four bonds broken due to the vacancy. P has an extra nuclear charge; hence, there are two electrons accomodated in its broken orbital with their spin paired off. Therefore, P does not form any bonds due to the vacancy. Two of the remaining silicon atoms form an electron pair bond, leaving an unpaired electron in the orbital of the last silicon atom [46]. The structure of the other E-centres are of the same type.

The formation of different types of P_nV_m, As_nV_m, etc. is possible. One suggested by Kortegaard Nielsen *et al.* [47] is an As_2V defect, with similar properties to P_2V.

4 Simulation program

Simulation programs based on physics provide the structure of the microelectronic device based on the given process steps. The commands are fed into the program as a sequence which corresponds to the real manufacturing process.

Since empirical modelling methods try to provide an analytical pattern or model for pre-existing data as simply as possible, physical modelling methods are based on pre-existing physical models. In this way the results are predictable, easy to obtain and cheaper than with the empirical modelling. However, the disadvantage of the physical modelling is that the information about the physics, mathematics, and chemistry must be already inserted in the program. This kind of program package already exists.

S is a modelling program package for semiconductor devices, made by Silvaco International Inc. It consists of several different parts. Two of the main parts are and which perform the actual modelling. In addition to these, supporting programs are included which simplify the usage of and , and help in analyzing the data. These programs are, T , D B , D E and O .

D B is an interface which helps with writing the code. T P is a program to plot out the results of simulations. T P can plot a picture of the device and the calculated data. One can also plot different types of schemes for the device, such as the current carrier distribution, the potentials and the doping concentrations [48].

4.1 Athena

A is a program used to define the structure of a model device and to modify it. It predicts the physical structure of the device from the steps of the defined process. The problem must be defined so that there is information about the original geometry of the device, process sequences (e.g. etching, implantation, diffusion, etc.) and the physical models that are needed. This constructs the device in detail. The underlying principle of is the same as in the real semiconductor manufacturing process; every step must be taken in the correct sequence. For example, if doping is the required procedure for a particular area, the the whole wafer must be oxidised. Subsequently, the oxygen layer is etched off from the areas, which are supposed to be doped. Only after this the actual doping can be done. Following doping, the whole oxygen layer is then etched off from

the wafer [49].

4.2 Atlas

A is a physics based 2D and 3D device modelling program which predicts the electrical behaviour of a semiconductor device structure, and provides visualization of the functional physics of the device.

A is intended to be used with VWF Interactive Tools which includes D B , T P , D E , M V , and O . A is most commonly used together with . The structure of the device is defined with , and the electrical properties are calculated using . The structure made with is used as an input for . The joint use of these two programs makes it possible to evaluate the effects of the process parameters on the final product.

Device simulators based on physics strive to reproduce the electrical properties of devices derived from their structure, physical properties, and applied bias settings. This is done by dividing the device up into cells or elements in two or three dimensions. The movement of the charge carriers can be simulated esentially by applying Maxwell's equations to each cell, while ensuring continuity.

A also enables the inclusion of defects in the simulations. In this way, the defects are represented as trap levels, and hence require the energy levels and capture cross sections for electrons and holes, concentration of the defects, and the degeneracy of the defects [48].

5 Simulations

The purpose of the simulations is to identify and specify the effects of radiation induced defects on the leakage current of the silicon based particle detectors. The goal is to create a model and validate the capability of present simulation packages to model radiation induced defects. In the case of reverse bias, the anode current is the leakage current of the diode.

The simulations are performed by simulating a diode-like structure with the S pro-gram package. A is used to create the diode at the start of each simulation. In this way, the structure can be modified in every simulation. Construction of the diode does not require much computing time. The defects are included after the manufacturing process in the part of the program, immediately before the electrical calculations. Hence, the defects are the ones that are introduced, and are not affected by the manufacturing process.

The electrical calculations simulate the application of a bias voltage to the diode A then calculates the currents in the electrodes. The simulations are employ a two dimensional model; therefore, the current calculated by is not the true current. These currents, which are recoded in a log file, are expressed in amperes per micron. Due to the 2D nature of the simulations, sets the third dimension to one micron. The real current value can be calculated by multiplying the log file current by the width of the device. The current density can then be calculated using the expression

$$J = \frac{I}{A}, \tag{24}$$

where I is the current and A is the area of the electrode. Here, A is the area of the bottom of the device.

5.1 Diode structure

The simulated structure of the detector is a simple p^+-on-n diode. The size of the two dimensional diode is 50×50 μm. The initial doping of the silicon wafer is done with phosphorous, at a concentration of 1×10^{13} cm^{-3}. This produces an n-type substrate. The p^+-type silicon is achieved by ion implantation with 1×10^{15} cm^{-3} dose of boron. The structure is illustrated in figure 8.

The doping profile of the simulated diode is seen in figure 9. The p^+ area is seen at the top of the diode, directly under the electrode. The p^+ doping is not very deep, but the doping depth can be calculated from equation (20).

Figure 10 shows the mesh used to define the structure and calculation points. It can be seen from the figure that the grid is a too sparse in the boundary regions, and near the p-n junction. This is discussed further in Section 7 Conclusions.

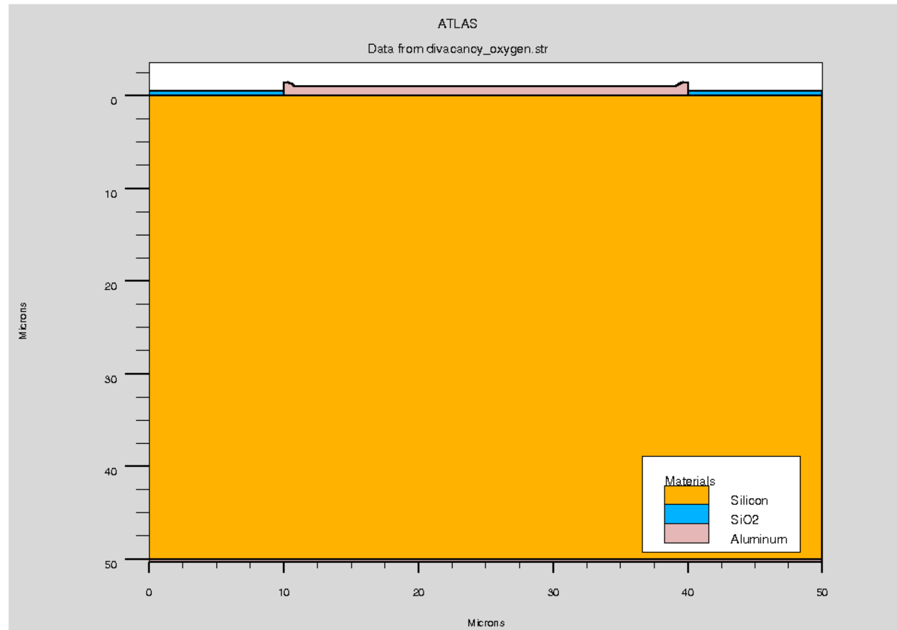

Figure 8: The structure of the simulated diode plotted with T P .

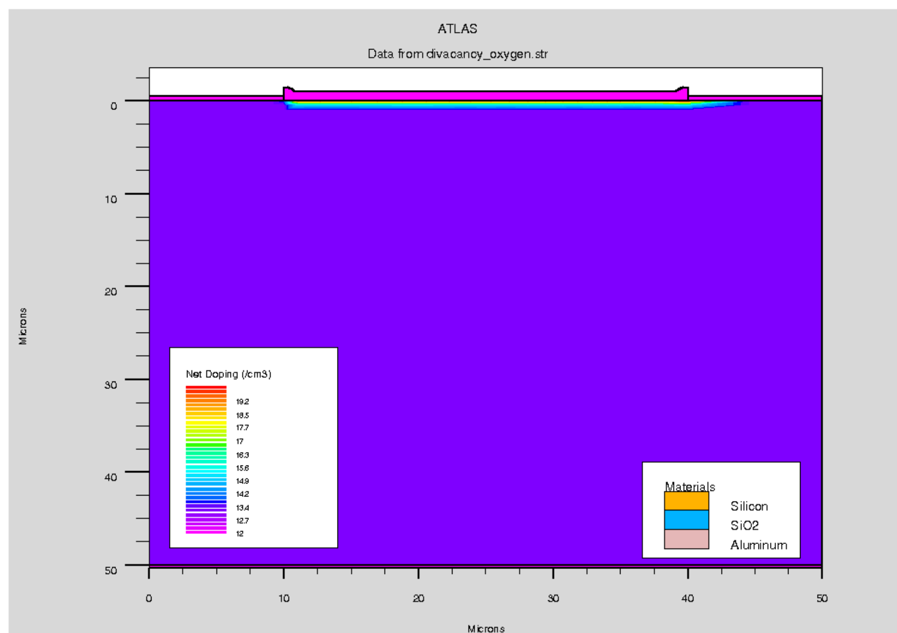

Figure 9: Doping profile of the simulated diode.

5.2 Defect parameters

The parameters used to simulate the defects are taken from either calculations or experimentals measurements of the chosen defects. The parameters required for the simulation

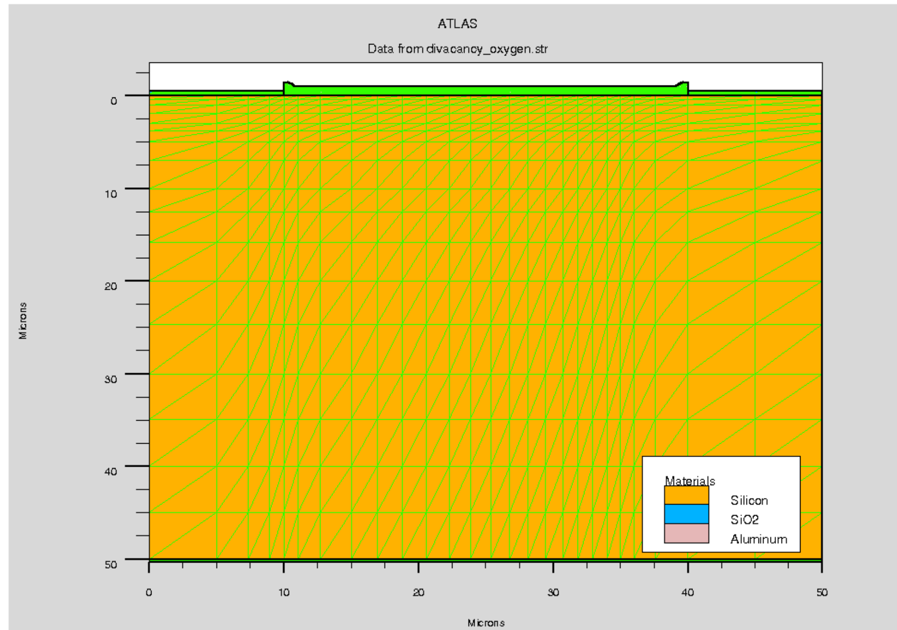

Figure 10: The mesh used to define the structure and calculation points of the diode.

are the energy levels, capture cross sections for electrons and holes, defect concentrations, and the degenerancy of the defect. Energy levels and concentrations are usually known; however, capture cross sections are somewhat harder to obtain. Several measurements have been performed to define the capture cross sections for electrons, or holes, but rarely for both. This causes another problem; namely, the compatibility of different studies with each other.

The defects are defined within the complete diode as traps, via a `trap` command, which requires energy level, type of the defect, capture cross sections for electrons and holes, concentration of the defects, and the degeneracy of the defect as input. In addition, the region to which the defects are introduced, can be specified; however, in this case, they are distributed over the whole diode. The simulation parameters are presented in table 1.

In the simulations, the defects are studied on an individual basis, with variable concentration. In this way, the dependence of the leakage current can be seen as a function of induced damage.

The parameters for the defects are taken from the literature. In addition, there are some estimations included in the capture cross sections and degeneracy of the defects. The degeneracy is estimated to be one for every defect, since there is no obvious reason or

Table 1: Parameters used for the defects in the simulations of leakage current. The type defines the reference band edge; acceptor energies are given with respect to the conduction band edge, E_C, donors are given respect to the valence band edge E_V, in electronvolts. Sign, and sigp are the capture cross sections for electrons and holes, respectivley.

Defect [Ref.]	Type	Level	sign	sigp	degen
VV [50]	Acceptor	0.42	2.00×10^{-15}	2.00×10^{-15}	1
VVV [50]	Acceptor	0.46	5.00×10^{-15}	5.00×10^{-14}	1
C_iO_i [50]	Donor	0.36	2.50×10^{-14}	2.50×10^{-15}	1
PV [45]	Donor	0.277	5.00×10^{-16}	5.00×10^{-16}	1
V_2O [24]	Acceptor	0.545	1.7×10^{-15}	9.0×10^{-14}	1
As_2V [47]	Donor	0.20	2.5×10^{-15}	2.5×10^{-15}	1

evidence to assume otherwise. The capture cross sections are usually given only for one of the charge carriers, hence the approximation for the cross sections.

6 Results

Results calculated in this work are sumarized by figure 11, where all the simulated defects are included. The leakage current is plotted against the bias voltage. The bias voltage is negative, due to the reverse bias of the diode. Note that the concentration of the defects varies from defect to defect. This is due to the fact that the effects of the defects differ greatly from each other; hence, it is not possible to plot them in the same graph for a single, fixed concentration.

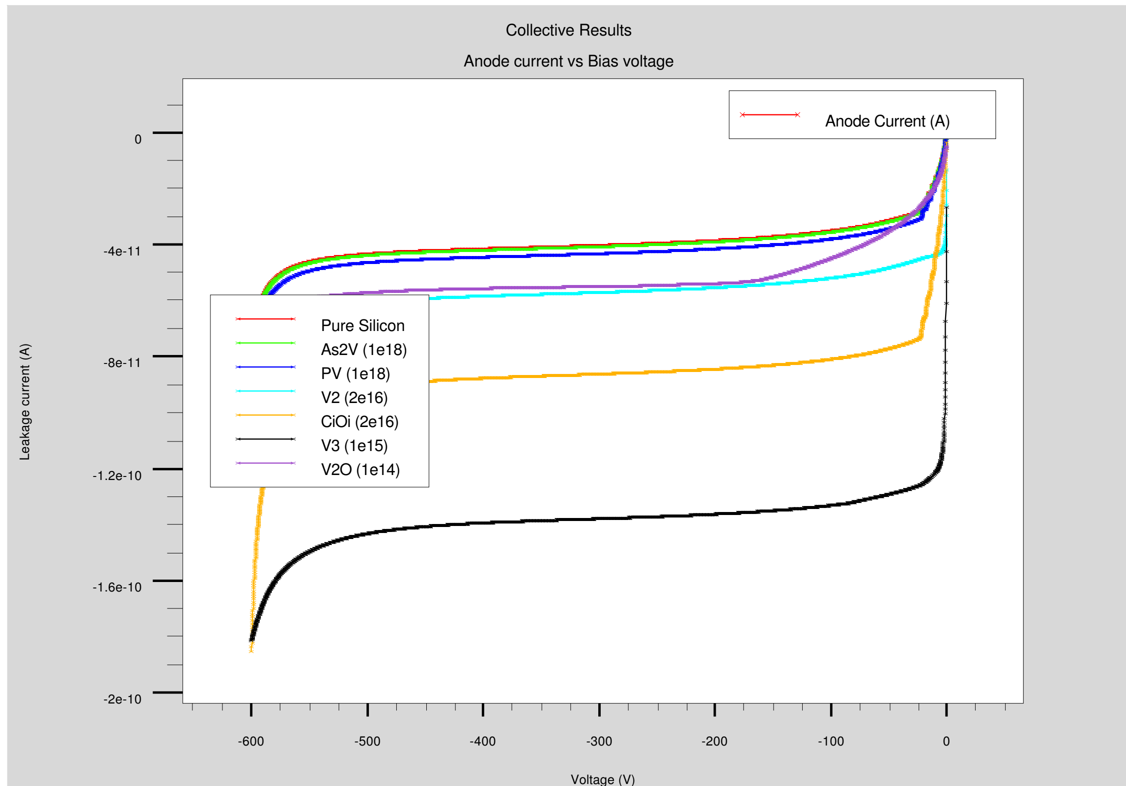

Figure 11: Collective plot of the leakage current against reverse bias voltage for all the simulated defects.

6.1 As_2V and PV

It can be seen from figure 12 that the As_2V defect is not particularly harmful. Even when the concentration of the defect is 1×10^{19} cm^{-3}, the increase in the leakage current is modest.

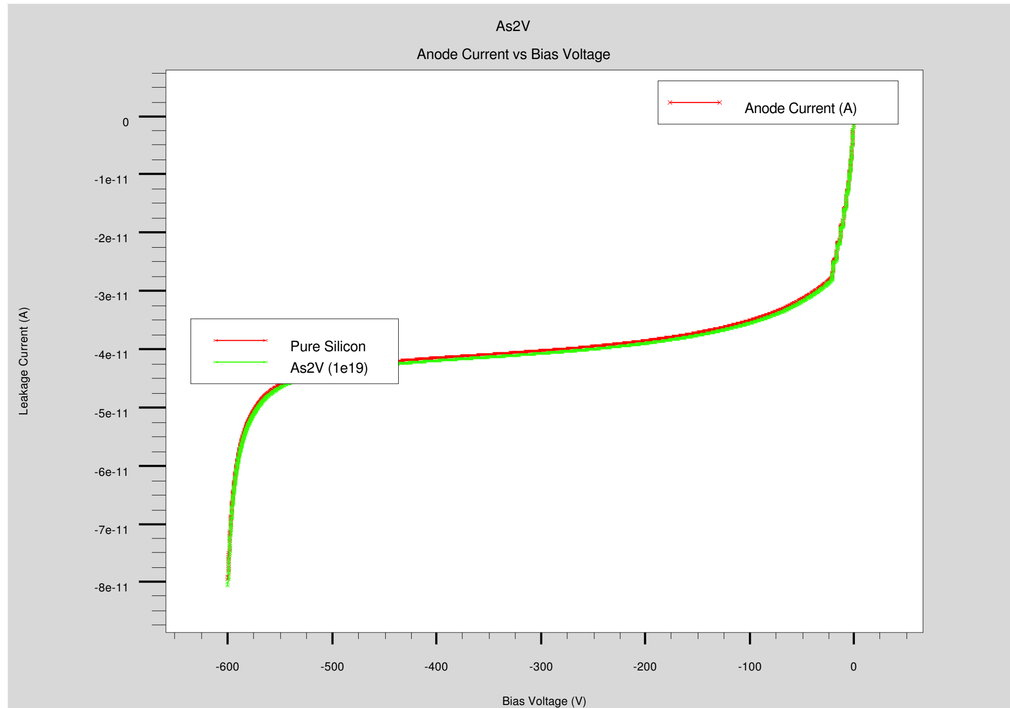

Figure 12: As_2V at high concentration, compared with pure silicon.

The same can been seen in figure 13, although it has to be noted, that the simulated state is only the donor state of the PV defects.

6.2 Divacancy and C_iO_i

The divacancy (figure 14), and C_iO_i (figure 15) complexes represent moderate damage in silicon. Their effect on the leakage current can be detected at relatively low defect concentrations, 1×10^{15} cm^{-3}.

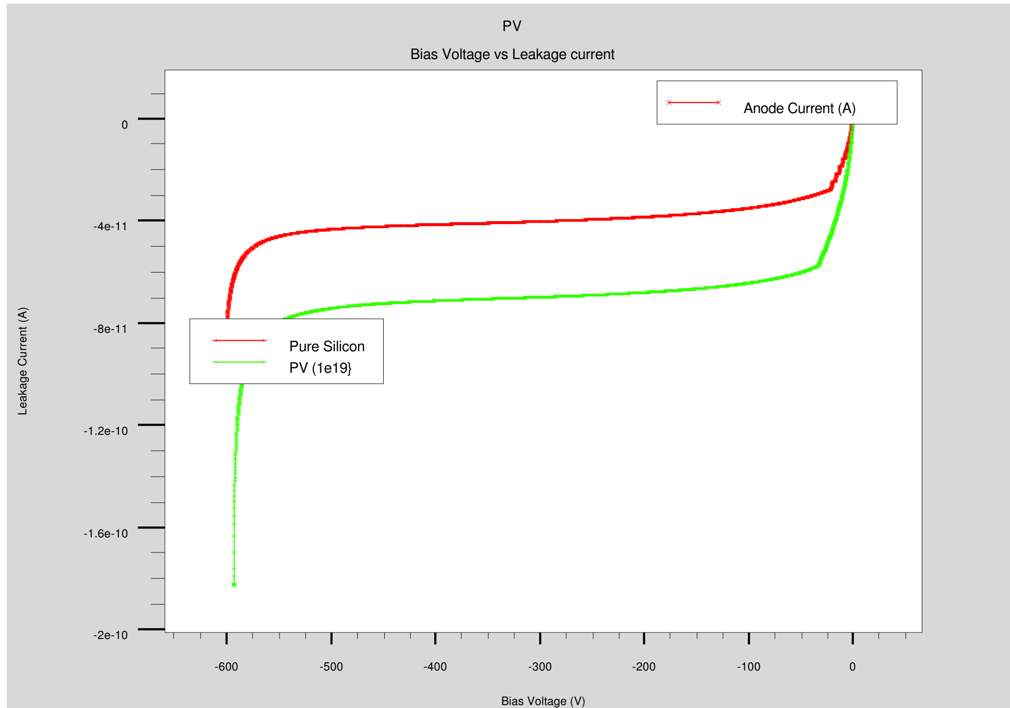

Figure 13: *PV* at high concentration, compared with pure silicon.

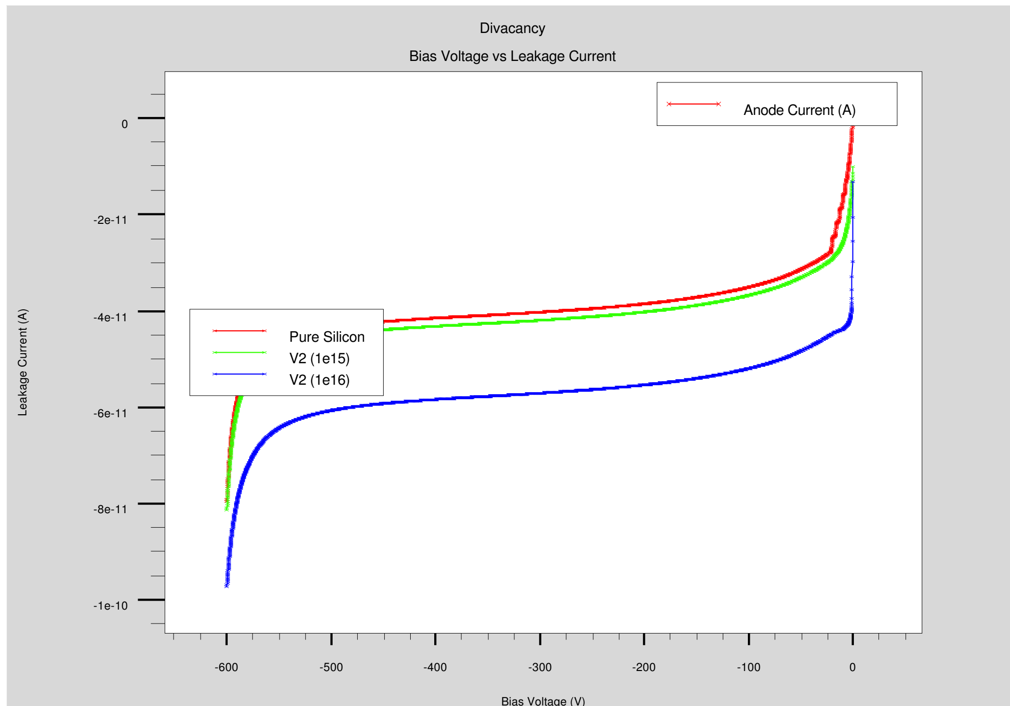

Figure 14: Divacancy results plotted with two different concentrations, and compared with pure silicon.

The behaviour of these two defects is similar considering the leakage current. The C_iO_i defect seems to cause slightly more leakage current.

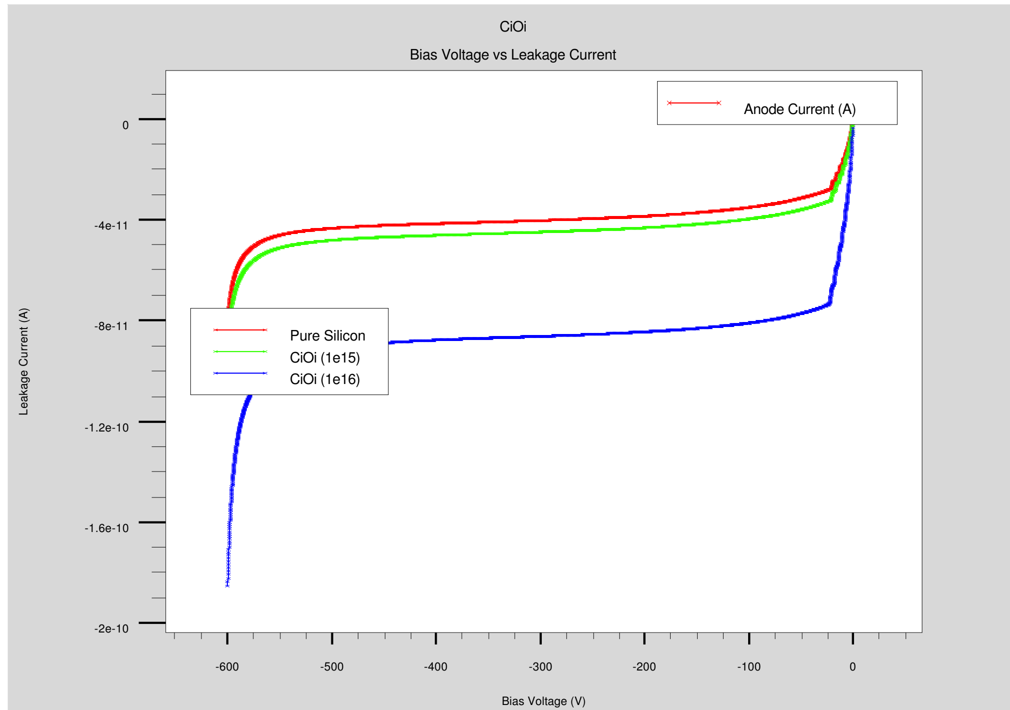

Figure 15: Simulation for the C_iO_i complex plotted with two different concentrations, and compared with pure silicon.

The results for C_iO_i are consistent with Moll *et al.* [51]. They state that the leakage current is almost independent of native defects.

6.3 Divacancy-Oxygen and trivacancy

Trivacancies V_3 (figure 16) and divacancy-oxygen (figures 17 and 18) can be considered the most harmful defects in this study. They start to affect the leakage current at relatively low concentrations, and the leakage current have an exponential behaviour as a function of concentration.

The trivacancy has not yet been identified experimentally; however, Ahmed *et al.* [29] have suggested it is present in neutron or proton irradiated *n*-type silicon.

In the case of divacancy-oxygen defects, increasing the concentration above 1×10^{14} cm^{-3} causes the diode to lose its diode-like behaviour. In other words, the *p*-*n* junction starts

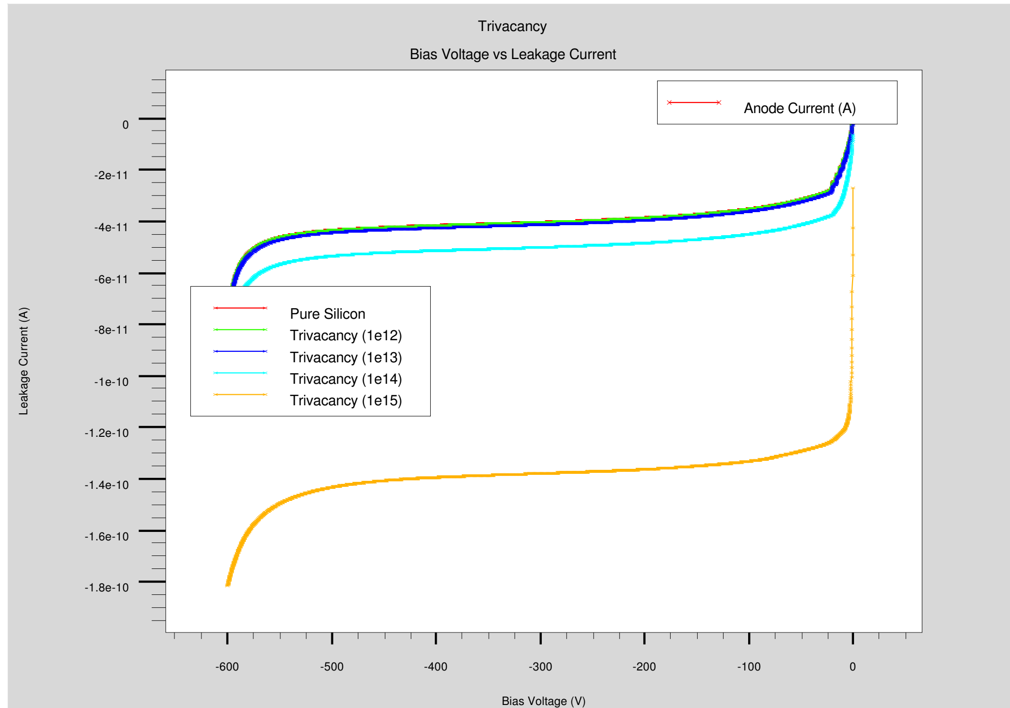

Figure 16: Trivacancy results plotted with four different concentrations, and compared with pure silicon.

to vanish (see figure 17). This can be due to the fact that the divacancy-oxygen complex also strongly affects the effective doping and may cause type-inversion.

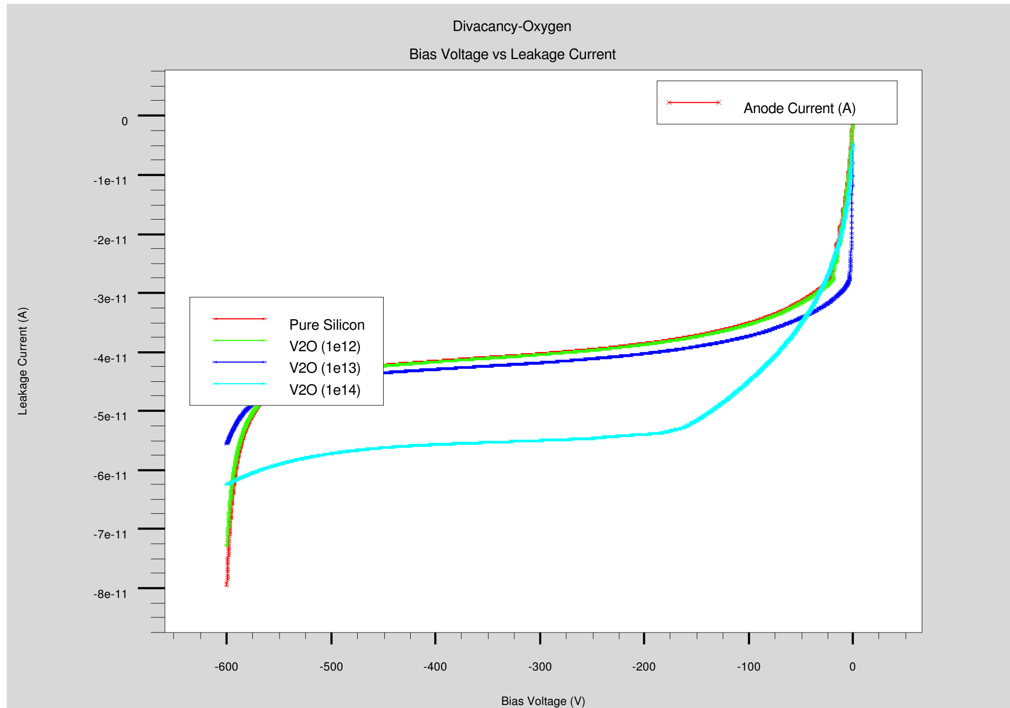

Figure 17: Divacancy-oxygen results plotted with four different concentrations, and compared with pure silicon.

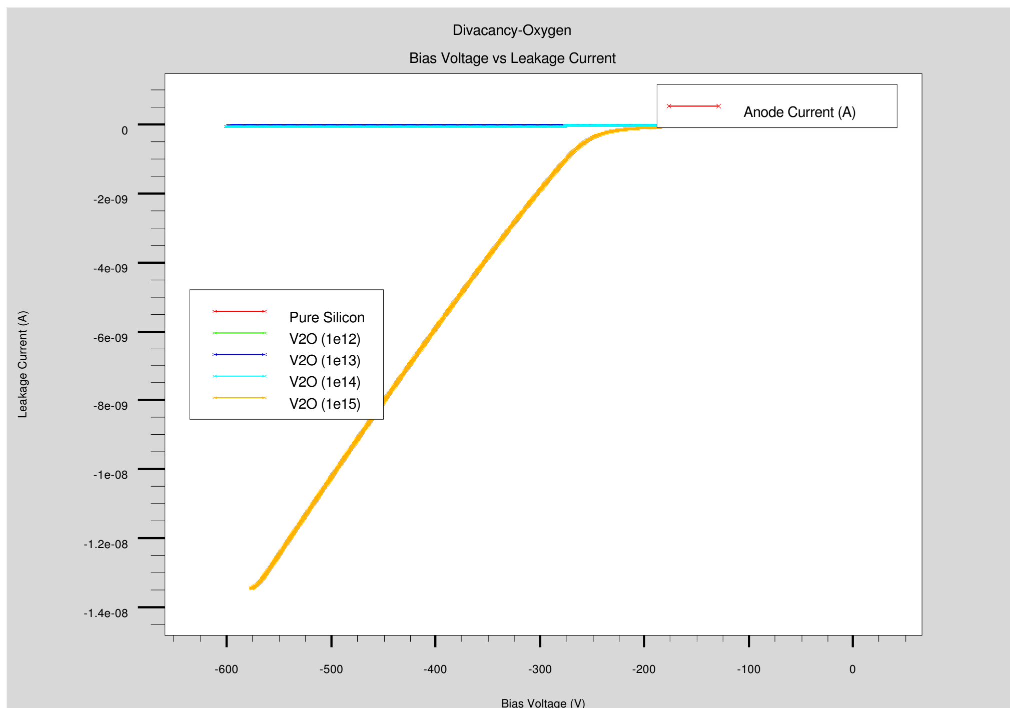

Figure 18: Divacancy-oxygen complex destroying the diode behaviour of the detector.

When the concentration of V_2O is $1{\times}10^{15}$ cm^{-3}, the behaviour of the diode is almost linear

at over −300 V (figure 18). This is strong evidence that the effective doping concentration is greatly diminished, and the diode-like behaviour has vanished.

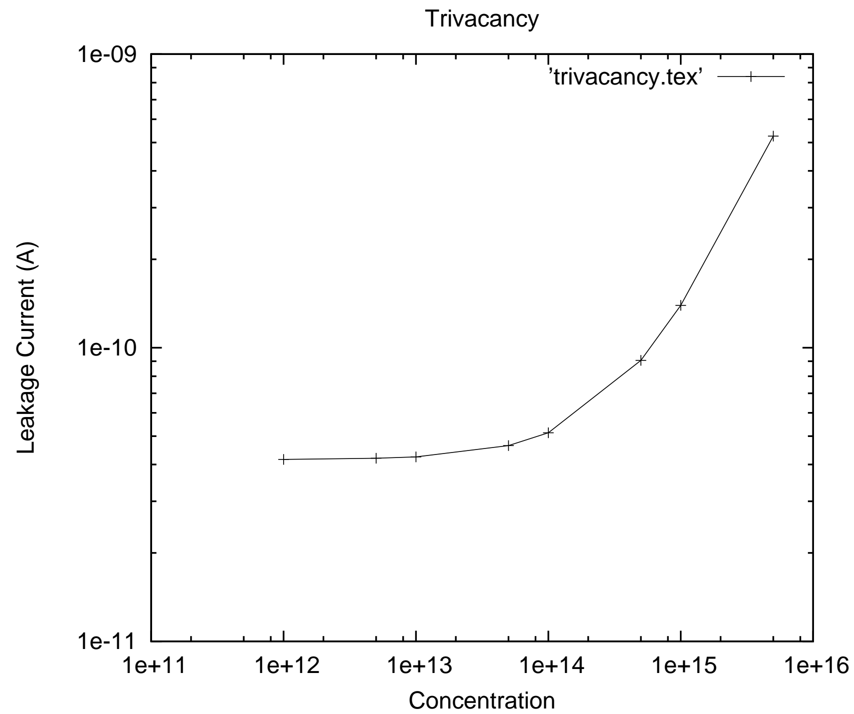

Figure 19: Leakage current caused by V_3 plotted against the defect concentration (cm^{-3}).

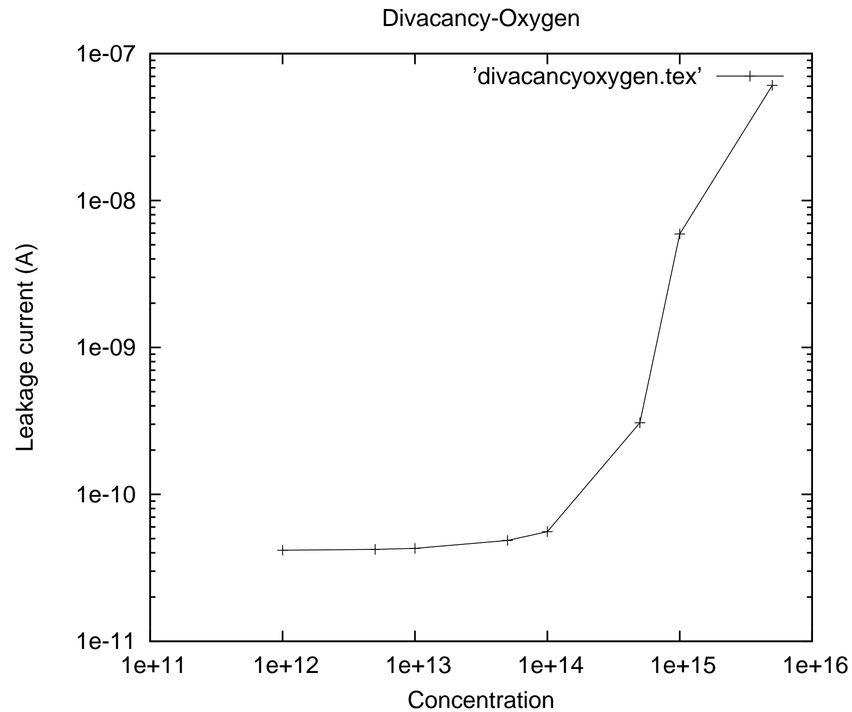

Figure 20: Leakage current caused by V_2O plotted against the defect concentration (cm^{-3}).

It can be seen in figures 19 and 20 that the effect of the trivacancies and divacancy-oxygen increases exponentially as a function of the concentration of the defects. This suggests that the detectors will deteriorate, due to the accumulation of the radiation induced defects over time.

In addition, these results suggests that oxygen atoms have a harmful effect on the silicon, with respect to the leakage current.

7 Conclusions

As seen in the figures from 11 to 20, the model predicts the behaviour of the leakage current correctly. Depletion, and breakdown voltage can be clearly seen from these plots. The model seems to be able to predict the type-inversion caused by the divacancy-oxygen complex, which is seen in figure 18.

The magnitude of the leakage current is greatly overestimated by the model. A real detector has a leakage current of the order of 1 μA, while the simulations give leakage currents

the order of 1 mA. This is assumed to arise from the structure of the detector used, and it is presumed to be only a biasing current; it has the same magnitude for each simulation. Therefore, the phenomena caused by the defects are considered to be realistic.

The biasing current is most likely to arise from the structure of the diode and the definition of the mesh. As seen in figure 10, the grid is too coarse at the edges of the device. This, combined with the boundary conditions, leads to incorrect simulation of the surface-to-edge-effects. In addition, the mesh could be denser in the vicinity of the *p*-doped region, near the *p*-*n* junction.

Another source of error is the structure of the diode. None of the methods to decrease the leakage current, or to smooth the applied electric field, have been implemented in this simulation, e.g. guard rings. This makes the leakage current for the present models larger.

One more source of error, which does not affect the same way as the previous ones, is the source of the information about the defects. The parameters required are not usually all from the same experiments, and thus there is a small margin for errors. Hence, one solution may be to employ *ab initio* calculations as a source for the parameters. This would provide an efficient, reliable way to explore different possibilities of material and defect engineering.

A more reliable way to study the effects could be to simulate only the bulk effects of the defects. This could be done by excluding the boundary conditions from the S software. Hence, the effects would be purely those in the doped silicon, and therefore the results would provide greater benefit in the development of the detectors.

In conclusion, the method used to simulate the effects of radiation induced defects essentially works as intended. However, further studies are needed to develop it into an efficient tool for engineering and design of real detectors.

REFERENCES

[1] http://rd50.web.cern.ch/rd50/, cited 31.8.2007.

[2] Atkins P.W., Physical Chemistry, 1978, Oxford, Oxford University Press, 1016 p. ISBN 0-19-855148-7.

[3] Callister W., 2003, Materials Science and Engineering an Introduction, 6.th edition, John Wiley & Sons inc., United States of America, 820 p., ISBN 0-471-22471-5.

[4] Sinkkonen J., 1996, Puolijohdeteknologian perusteet, Helsinki, 306 p., ISBN 051-22-3242-1.

[5] Ashcroft N. and Mermin N.D., 1976, Solid State Physics, London, Thomson Learning, 823 p. ISBN 0-03-083993-9.

[6] Grönlund T., 2007, Development of advanced silicon radiation detectors for harsh radiation environment, Lappeenranta, Acta Universitatis Lappeenrantaensis 297, 82 p., ISBN 978-952-214-518-5.

[7] Fleta C. *et al.*, Simulation and test of 3D silicon detectors, Nuclear Instruments and Methods in Physics Research A 597, 642 (2007).

[8] Kok A. *et al.*, 3D detectors - State of the art, Nuclear Instruments and Methods in Physics Research A 560, 127 (2006).

[9] Eremin V. *et al.*, Current injected detectors at super-LHC program, Nuclear Instruments and Methods in Physics Research A 583, 91 (2007).

[10] Leinonen K., 2006, Fabrication and characterization of silicon position sensitive particle detectors, Lappeenranta, Acta Universitatis Lappeenrantaensis 235, 91 p., ISBN 952-214-141-0.

[11] Knoll G., 2000, Radiation detection and measurement, 3rd edition, John Wiley & Sons Inc., United States of America, 802 p., ISBN 0-471-07338-5.

[12] Agram J.-L. *et al.*, The silicon sensors fo the Compact Muon Solenoid tracker - design and qualification procedure, Nuclear Instruments and Methods in Physics Research A 517, 77 (2004).

[13] Civinini C., The CMS Silicon Strip Tracker, Nuclear Instuments and Methods in Physics Research A 579, 726 (2007).

[14] Kremmer C. *et al.*, Strip detectors, United States Patent No. US 6,184,562 B1, February 2001.

[15] Allkofer Y. *et al.*, Design and performance of the silicon sensors for the CMS barrel pixel detector, Nuclear Instuments and Methods in Physics Research A 584, 25 (2008).

[16] MacEvoy B.C., Defect kinetics in novel detector materials, Materials Science in Semiconductor Processing 3, 243 (2003).

[17] Watkins G.D. and Corbett J.W., Defects in Irradiated Silicon. I. Electron Spin Resonance of the Si-A Center, Physical Review 121, 1001 (1961).

[18] Corbett J.W. and Watkins G.D., Silicon Divacancy and its Direct Production by Electron Irradiation, Physical Review Letters 7, 314 (1961).

[19] Watkins G.D. and Corbett J.W., Defects in Irradiated Silicon: Electron Paramagnetic Resonance of The Divacancy, Physical Review 138, A 543 (1965).

[20] Watkins G.D., Intrinsic defects in Silicon, Materials Science in Semiconductor Processing 3, 277 (2000).

[21] Baraff G.A., Silicon Vacancy: A Possible "Anderson Negative-*U*" system, Physical Review Letters 43, 956 (1979).

[22] Latham C.D. *et al.*, Electronic structure calculations for substitutional copper and monovacancies in silicon, Physica Scripta T126, 61 (2006).

[23] Stallinga P. *et al.*, Microscopic identification and electronic structure of a dihydrogen-vacancy complex in silicon by optical detection of magnetic resonance, Physical Review Letters 80, 422 (1998).

[24] Pintilie I. *et al.* Second-order generation of point defects in gamma-irradiated float-zone silicon, an explanation for "type inversion", Applied Physics Letters 82, 2169 (2003).

[25] Öğüt S. and Chelikowsky J.R., Large Pairing Jahn-Teller Distortions Around Divacancies in Crystalline Silicon, Physical Review Letters 83, 3852 (1999).

[26] Öğüt S. and Chelikowsky J.R., *Ab initio* investigation of point defects in bulk Si and Ge using cluster method, Physical Review B 64, 245206 (2001).

[27] Monakhov E.V. *et al.*, Formation of a double acceptor center during divacancy annealing in low-doped high purity oxygenated Si, Physical Review B 65, 233207 (2002).

[28] Makhov D.V. and Lewis L.J., Stable Fourfold Configurations for Small Vacancy Clusters in Silicon from *ab initio* Calculations, Physical Review Letters 92, 255504 (2004).

[29] Ahmed M. *et al.*, Deep-level transient spectroscopy studies of silicon detectors after 24 GeV proton irradiation and 1 MeV neutron irradiation, Nuclear Instruments and Methods in Physics Research A 457, 588 (2001).

[30] Bleka J.H. *et al.*, Room-temperature annealing of vacancy-type defect in high-purity *n*-type Si, Physical Review B 76, 233204 (2007).

[31] Estreicher S.K. *et al.*, The ring-hexavacancy in silicon: A stable and inactive defect, Applied Physics Letters 70, 432 (1997).

[32] Hastings J.L. *et al.*, Vacancy aggregates in silicon Physical Review B 56, 10215 (1997).

[33] Chadi D.J. and Chang K.J., Magic number for vacancy aggregation in crystalline silicon, Physical Review B 38, 1523 (1988).

[34] Pesola M. *et al.*, Computational study of interstitial oxygen and vacancy-oxygen complexes in silicon, Physical Review B 60, 11449 (1999).

[35] Coutinho J. *et al.*, Oxygen and dioxygen centers in Si and Ge: Density-functional calculations, Physical Review B 62, 10824 (2000).

[36] Lindström J.L. *et al.*, The VO_2^* defect in silicon, Physica B 340-342, 509 (2003).

[37] Fretwurst E. *et al.*, Recent advancements in the development of radiation hard semiconductor detectors for S-LHC, Nuclear Instrument and Methods in Physics Research A 552, 7 (2005).

[38] Boisvert V. *et al.*, Characterization of oxygen dimer-enriched silicon detectors, Nuclear Instruments and Methods in Physics Research A 552, 49 (2005).

[39] Bruzzi M. *et al.*, Thermal donor generation in Czochralski silicon particle detectors, Nuclear Instruments and Methods in Physics Research A 568, 56 (2006).

[40] Pintilie I. *et al.*, Stable radiation-induced donor generation and its influence on the radiation tolerance of silicon diodes, Nuclear Instruments and Methods in Physics Research A 556, 197, (2006).

[41] Stolk P.A. *et al.*, The effect of carbon on diffusion in silicon, Materials Science and Engineering B36, 275 (1996).

[42] Hönniger F. *et al.*, DLTS measurements of radiation induced defects in epitaxial and MCz silicon detectors, Nuclear Instruments and Methods in Physics Research A 583, 104 (2007).

[43] Londos C.A., Capacitance transient studies of a metastable defect in silicon, Physical Review B 34, 1310 (1986).

[44] Zangenberg N. *et al.*, On-line DLTS investigation of mono- and di-vacancy in *p*-type silicon after low temperature electron irradiation, Nuclear Instruments and Methods in Physics Research B 186, 71 (2002).

[45] Nylandsted Larsen A. *et al.*, *E* Center in silicon Has a Donor Level in the Band Gap, Physical Review Letters 97, 106402 (2006).

[46] Watkins G.D. and Corbett J.W., Defects in Irradiated Silicon: Electron Paramagnetic Resonance and Electron-Nuclear Double Resonance of the Si-*E* Center, Physical Review 134, A1359 (1964).

[47] Kortegaard Nielsen H. *et al.*, The As_2V complex in silicon: Band-gap levels, migration and annealing, Nuclear Instruments and Methods in Physics Research B 253, 172 (2006).

[48] SILVACO International inc., ATLAS User's Manual, Santa Clara, 898 p., www.silvaco.com.

[49] SILVACO International inc., ATHENA User's Manual, Santa Clara, 434 p., www.silvaco.com.

[50] Petasecca M. *et al.*, Numerical simulation of radiation damage effects in *p*-type silicon detectors, Nuclear Instruments and Methods in Physics Research A 563, 192 (2006).

[51] Moll M. *et al.*, Leakage current of hadron irradiated silicon detectors: material dependence, Nuclear Instruments and Methods in Physics Research A 426, 87 (1999).